Expanding Insight into One to One foaming

A study into a Novel Fabrication Method of Midsoles for Athletic Footwear based on INFUSE™ Olefin Block Copolymers

van Lange, S.G.M.

Award date:
2020

Expanding Insight into One to One foaming

A study into a Novel Fabrication Method of Midsoles for Athletic Footwear based on INFUSE™ Olefin Block Copolymers

Sophie van Lange

May 2020

Author: S.G.M. (Sophie) van Lange

StudentID: 1371924
Email: s.g.m.v.lange@student.tue.nl
Supervisor: Prof. dr. ir. C.F.J. den Doelder
Affiliation: Laboratory of Physical Chemistry – Department of Chemical Engineering and Chemistry
Eindhoven University of Technology
5600 MB Eindhoven, The Netherlands

Project coach: Dr. J.J. van Dun
Dr. M.A. Prieto
Affiliation: Packaging and Specialty Plastics (P&SP)
Dow Europe GmbH
8810 Horgen, Switzerland

Abstract

Significant automation of advanced manufacturing techniques of athletic midsole foams is required to meet the global demand of athletic footwear. INFUSE™ OBC, a polyethylene-based Olefin Block Copolymer resin is expected to yield the best midsole performance of the available polyolefin-based elastomers, as well as lifetime due to its favorable elastomeric properties. In the current state of the art, production of such midsoles requires significant manual intervention. Using a 'One to One' foaming technique, the foam is expected to grow to its final dimensions inside a mold cavity upon injection, a first step necessary for further automation of the shoe manufacturing process. The work presented here lays the foundation of the development of such a processing method by providing the first experiments of constrained foaming of modified OBC materials.

By analyzing the shear and extensional rheology, as well as the peroxide crosslinking kinetics, the viscoelastic requirements for foam stability are clarified in the context of the employed methods. Based on the generation of a specified foam density and cell size distribution, a foaming window was defined by employing a found correlation between the extensional and shear rheology of OBC. This leads to a direct comparison of the conventional method of Crosslinked Injection Molding and the first experiments of One to One foaming. The effect of the methodology on the foam structure is studied with a microscopy analysis, in combination with an automated image analysis tool. The average cell size was observed to increase with increasing compound viscosity, and the magnitude and distribution were observed to be higher for One to One foamed samples. Additional mechanical properties such as compression set, split tear and hardness were recorded in order to make a prediction for the necessity of a post-crosslinking step with silane chemistry for lightly crosslinked and thermoplastic formulations. Hardness was demonstrated to depend linearly on the foam density, and compression set was overall observed to be very low. The split tear was evaluated to potentially be improved by a post-crosslinking step, though the methodology of One to One foaming had not impaired the performance with respect to the traditional foaming method.

Contents

1 Introduction

Inspired by naturally occurring materials such as cork, sponge and coral, man has been motivated to manufacture synthetic versions of cellular materials, better known as foams. Foam popularity can be attributed to their excellent insulating, thermal and acoustic properties, pleasant touch in combination with their light weight and interesting mechanical properties depending on the gas fraction and cell size distribution [1]. Foam properties can be tailored to meet particular performance requirements by careful selection of the raw materials, additives and processing conditions. Foamed plastics can be flexible, rigid, high or low density, and can have open or closed voids. The creation of a low density foam with simultaneous advantageous mechanical properties would provide both environmental and economic benefits.

Decades of research have enlightened much of the thermodynamics of aqueous foams, which often find their application in food and cosmetics. However, many other everyday materials contain polymeric foams that have relatively unexplored properties. These polymeric foams can be made from various different polymers and are abundant in materials for furniture, packaging, construction, insulation, textile and automotive applications [2]. Amongst those applications, footwear is one of the largest consumer markets of synthetic polymers of about 5 million tons per year, of which approximately 7% is used in foamed midsoles for athletic shoes. **Figure 1** demonstrates the components of a running shoe, including the shoe upper, insole, midsole and outsole structure. The nature and morphology of the foams used in midsoles have a direct impact on the footwear comfort, resilience, durability, stability, light weight, impact absorption and aesthetics [3], hereby providing a range of benefits to end customers.

Figure 1: Different components of the soling in athletic footwear.

1.1 Polymers in midsole foams

Advanced performance, excellent processability, and cost effectiveness are the major driving forces in footwear foam innovations. The development of synthetic polymers during the last century drove the replacement of natural materials such as leather in athletic footwear due to their economic benefits. Early applications of polymers in footwear soling consisted of compression molded rubber soles, which were cured at high temperatures. Also plasticized

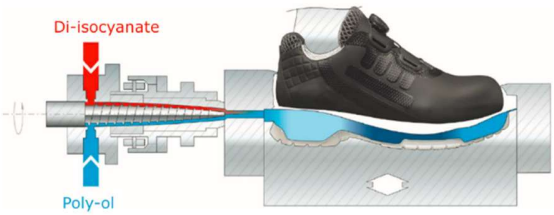

Figure 2: Automated injection process of PU midsoles.

polyvinyl chloride (PVC) was commonly applied, which resulted in relatively dense but flexible soles with a rubbery feel.

Elastomers, a class of high molecular weight polymers that behave elastically above their T_g, were found to provide the best cushioning and resiliency in midsole foams. The elasticity of elastomers is entropy-driven, meaning that they naturally recover to their equilibrium 'entangled random coil' state once an imposed stress is removed.

With the development of polyurethane elastomers (PU), foaming and automated processing of midsole foams became common practice, yielding lightweight midsoles. As a result of the intrinsic polarity of PU and the low-viscous nature of the mix, a polyol and di-isocyanate can be readily injected and foamed between the outsole and the upper by making use of surfactant stabilization [4]. This process is schematically shown in **Figure 2**. This resulted in an effective automatized processing technique for thermoplastic PU foams which can be foamed to relatively low densities of 0.5 g/cm^3-0.35 g/cm^3 in the presence of surfactant while still maintaining a rubbery touch. Despite the favorable processing capabilities, PU is intrinsically limited due to its UV and hydrolytic sensitivity, which leads to rapid discoloration and weathering issues [5].

Polyolefin elastomers (POEs) prove to be suitable competition for applications in footwear as they do not exhibit the intrinsic sensitivities of PU foams. POE is a product family produced with ethylene and α-olefins. By development of new metallocene catalyst systems, the polymer structure could be modified with branching, and the crystallinity, density and molecular weight distributions could be controlled [6]. These developments lead to the fabrication of soft polyethylene-based polymers with high flexibility and good elastomeric properties [6].

Also ethylene vinyl acetate copolymers (EVA) have long been the benchmark in footwear applications (**Figure 3**). Approximately 59% of midsoles are currently made of EVA [7]. EVA can be foamed to relatively low densities (<0.3 g/cm^3) compared PU or PVC and the mechanical properties and foaming window of EVA are attractive.

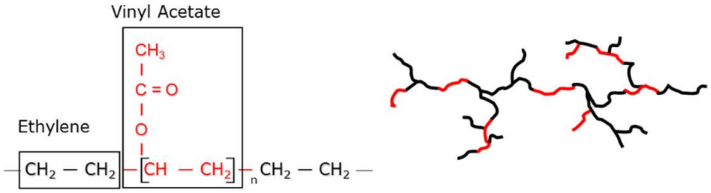

Figure 3: Chemistry and schematic representation of Ethylene Vinyl Acetate (EVA).

In order to further meet the performance demand of athletic footwear manufactures and consumers, INFUSE™ Olefin Block Copolymers (OBC) were tested and implemented in footwear formulations. This polymer has the unique architecture of both semi-crystalline 'hard' ethylene blocks, interchanged by elastomeric 'soft' ethylene-octene blocks (**Figure 4**). The large crystalline domains provide a relatively high melting point, but also improve the mechanical properties to outperform EVA in compression set and abrasion resistance. The amorphous domains provide better elasticity which contributes to the resiliency. These advantageous properties improve durability, flexibility and damping properties in sports shoes. In traditional foaming methods of polyolefin elastomers, addition of a crosslinking agent such as a peroxide is still necessary to yield foams with suitable aesthetics and performance [8].

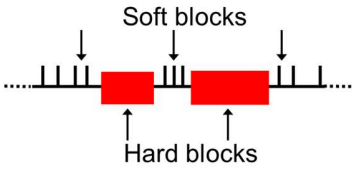

Figure 4: Schematic representation of INFUSE™ Olefin Block Copolymers. Soft blocks consist of ethylene-octene which prevents crystallization, the hard ethylene blocks can form lamella, resulting in crystallized domains.

1.2 Processing capabilities and perspectives

An estimated 83% of athletic shoe manufacturing sites reside in Asia, mainly in China and Vietnam. Since labor is becoming increasingly expensive in eastern countries, and the global drive towards sustainability is thriving, there is a pushing ambition of the industry towards automated production of shoes globally. Large athletic shoe brand owners have also expressed their wish to significantly automate their midsole production manufacturing to minimize cost and waste production [9]. Despite the advantageous foam quality and performance, OBC foams are currently limited in their automation capabilities [10].

1.2.1 **Crosslinked Injection Molding**

The conventional injection method for POE-and OBC-based materials is called 'Crosslinked Injection Molding' (CIM), of which the setup is schematically shown in **Figure 5**. Here, a polymer with its additives (blowing- and crosslinking agents, filler, pigments, etc.) are fed in a single screw injection unit. The temperature of the barrel is set above the melting point of the polymer, but below the temperature where curing and foaming might take place, typically 90-95 °C. The uncured and un-foamed polymer melt is then injected into a heated mold, often aided by pulling a vacuum on the mold interior. There, peroxide crosslinking and foaming agent decomposition occur under pressurized conditions and above the decomposition temperature of the blowing agent and crosslinking agent. Upon pressure release by opening of the mold the foam expands

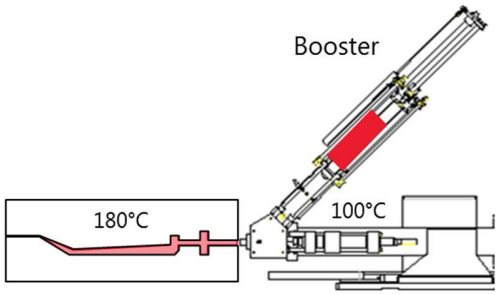

Figure 5: Crosslinked Injection Molding. A polymer mixed with crosslinking agent, blowing agent and other additives is injected into a hot mold. Crosslinking and decomposition of the blowing agent occurs. Upon opening of the mold, the midsole expands to its final dimensions.

to its final dimensions, often ejecting from the mold [9]. The midsoles have to be manually recovered and are then manually adhered to the remaining upper and outsole of the shoe, which is a time consuming and labor-intensive procedure. Besides the lack of automation perspective, the use of chemical blowing agents is no longer preferential. The research of physical foaming capabilities is currently insufficient due to the lack of available machinery.

1.2.2 **One to One foaming**

Considering the market for POEs in footwear, there is an opportunity to develop a process that allows the midsole to be directly injected in between the outsole and upper of the shoe to directly eliminate a large part of the manual labor in footwear manufacturing. The foam will then expand to its final dimension inside a mold cavity.

This technique should allow for automated production of athletic footwear as no manual adhesion step would be required after foaming, hence the name 'One to One Foaming'. This method would require a foam to be formed inside a mold. If the melt is injected into the mold, the pressure drop between the injection unit and the mold would provide the thermodynamic instability required for bubble nucleation. Alternatively, gas-laden pellets can be pre-loaded into the mold also. The foaming can be initiated by making use of chemical or physical blowing agents (paragraph 2.1), though physical foaming might be desired due to the possibility to foam at relatively low temperatures. It is expected that the polymer melt should be sufficiently stable during foaming while also remaining plastic enough to replicate the shape of an intricate mold. This behavior requires tailoring the formulation and the processing conditions. It is expected that a moderate amount of peroxide modification (crosslinking) is required to provide the extensional properties for foam formation while retaining the polymer's thermoplasticity, i.e. a fully crosslinked network has not been formed. One to One Foaming can then potentially make use of a dual-curing system (**Figure 6**), where these initial low levels of curing provide the rheological properties needed for foam stability while retaining thermoplasticity for injection. The finalized foam can subsequently undergo a post-crosslinking step if the mechanical properties that are required for optimal midsole performance are insufficient. While the first crosslinking step could be provided by

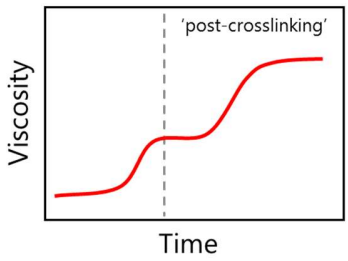

Figure 6: Viscosity evolution in a dual-curing system. The foaming action is indicated by the dashed line.

different types of crosslinking agents, such as peroxide or silane, the second step is desirably provided by silane-curing, as then no further heating of the foam is required, and crosslinking can proceed in the presence of an externally provided water source.

1.3 Hypotheses and research goals

The currently limited understanding of the foaming behavior of thermoplastic and lightly crosslinked foams obstructs the development of processing techniques that allow for automated processing of OBC-based foams. This work should lay the foundations for the development of One to One Foaming. It is hypothesized that OBC can be One to One Foamed at considerably lower curing levels than applied in traditional foaming methods. This foaming can potentially occur at lower processing temperatures in combination with physical blowing agents such as CO_2 or N_2. At these low temperatures, foam growth can be stabilized through modification of the polymer to improve the extensional viscosity as a result of long chain branching. It is furthermore hypothesized that post-crosslinking of this foamed structure can successfully occur to provide the final mechanical properties.

This work aims to defining a foaming window for OBC based materials from a rheological perspective, as well as studying the performance of such One to One foamed to evaluate the necessity of a post-crosslinking step.

The main research goals are:

Defining the curing kinetics of peroxide modification of two OBC materials differing in melt index with a Rubber Processing Analyzer (RPA) at different temperatures. This provides an understanding for the required conditions to achieve full curing at different temperatures and peroxide concentration.

Elucidating the shear rheological behavior of the modified material by Dynamic Mechanical Analysis (DMA). This involves acquiring information on η*, G', G" and tanδ at different peroxide loadings, temperatures and shear rates. This should aid in defining a foaming window of OBC for the employed processing methods; it is hypothesized that the optimal foam quality and properties correspond to a defined region in the polymer's viscoelastic behavior. There is thus sought after a viscosity that is representative for foaming processes, which are typically dominated by extensional properties.

Characterization of the extensional properties of the modified material at different temperatures and strain rates. This is combined with the shear rheology at the same temperatures to allow for a description of the strain hardening behavior and extensional viscosities at different peroxide levels.

Experimental development of One to One Foaming and exploration of physical foaming by creating foams in a constrained environment. Physical foaming will be approximated by first activating a chemical blowing agent above its decomposition temperature and to then cool the melt to the temperature of foaming. Samples prepared by conventional Crosslinked Injection Molding of equivalent formulations act as reference.

Characterization of the foam properties in terms of their morphology and mechanical properties. This involves imaging the bubbles by confocal microscopy and consequently measuring the cell size, cell size distribution and anisotropy. Additionally, other foam properties such as density, hardness, compression set, split tear and rebound resilience are characterized. This allows for comparison of traditionally foamed materials to One to One foamed equivalents.

Validation of the silane post-cure. It is hypothesized that after foaming of thermoplastic or moderately crosslinked INFUSE™ OBC, the performance requirements for midsole foams can be met by providing additional mechanical properties upon post-curing with silane chemistry. The characterization of the foam performance gives insight into the necessity of such a step.

2 Background on foams

In this chapter, the general information required for understanding foaming is introduced. This includes the typical components of a formulation for polymer foaming, but also the processes and dynamics that define a foaming experiment. Besides the typical ingredients and events that play a role in foam processing and stability, the performance requirements for athletic midsole applications will be reviewed.

A foam is a two-phase cellular system in which gas bubbles are enclosed in a liquid or solid medium. The creation of a polymeric foam requires the generation of gaseous bubbles in a polymeric continuous phase. The bubbles are separated by thin films (lamella) of polymer. The transition zones between a bubble and its neighboring bubbles are called 'plateau borders' and a junction of more than three plateau borders is called a vertex (**Figure 7**). Foams that have openings in their films through which the bubbles are interconnected are called 'open cell foams'. Foams for footwear applications are desired to have closed cells to prevent water penetration into the midsole.

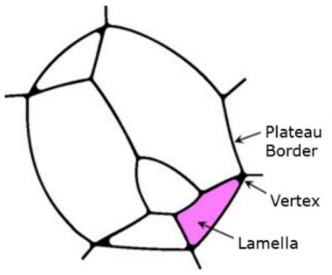

Figure 7: Foam structure. (Zabler et al. 2014)

2.1 Blowing agents

Creating porosity in a material is an energy intensive process due to the creation of many gas/liquid interfaces. The energy required to induce a blowing action can be supplied in various ways. The use of chemical blowing agents (CBAs) and physical blowing agents (PBAs) are the most commonly employed methods.

2.1.1 **Physical blowing agents**

Physical foaming typically occurs by mechanical incorporation of gas in a continuous phase. PBAs are typically gases that can be supplied directly into a polymer melt during extrusion or injection molding. Usually, foaming is initiated by inducing changes in phase behavior depending on the processing temperature and pressure of a polymer melt that is supersaturated with an inert gas [1]. Commonly used PBAs include inert gases such as CO_2 and N_2, but also water, fluorocarbons and volatile organic chemicals can be used [11]. Materials can be foamed with inert gases in an autoclave or using a gas injection unit.

Physical foaming is a relatively expensive process and is not commonly applied in the footwear industry since current injection molding machines are not typically equipped with a gas injection

unit. However, the usage of physical blowing agents is preferred as it can be used at lower processing temperatures than typical for CBAs, and does not contaminate the product with any residual CBA decomposition residues. These advantageous properties of physical blowing agents drive the industry to invest in research and development of physical foaming methods. The resources to do physical foaming are not always available.

Addition of a physical blowing agent is typically associated with a decrease of the viscosity of the polymer, this effect is often referred to as 'plastization'. Processing of polymers concentrated with PBAs can usually occur at relatively low temperatures [12].

2.1.2 **Chemical blowing agents**

Besides the ability to foam by direct supply of a gas, the gas can also be provided by the decomposition of a chemical compound. Blowing of a polymer with chemical blowing agents (CBAs) occurs through the formation of gas upon decomposition at elevated temperatures, often nucleated around its own decomposition remains or added nucleating agents [13]. A distinction can be made between endothermic and exothermic blowing agents [14]. The industry tends to drive away from the large-scale use of chemical blowing agents due to the liberation of odors and residuals. Besides, the decomposition kinetics are strongly temperature dependent, and there is an offset of decomposition, which is called the decomposition temperature. This requires the material to be heated above the decomposition temperature of the CBA prior to foaming. If foaming occurs at this high processing temperature, the mechanical properties of the polymer can be impaired. Besides, it is energy intensive and time inefficient.

A commonly used (exothermic) chemical blowing agent is azodicarbonamide (Azo) (**Figure 8**), of which the decomposition follows several pathways, ultimately releasing N_2 (62 wt%), CO (35 wt%), CO_2 (3 wt%) and ammonia in the gas phase [3, 15]. Although the gas generation of Azo has been studied extensively, the research community remains indecisive about the decomposition pathway. It is known that, besides the liberated gaseous compound, approximately 40% of the residue comprises solid material. Azo typically decomposes at 210 °C and has a gas yield of approximately 220 cm^3/g. Exothermic blowing agents typically have a relatively narrow decomposition temperature range, and they are autocatalytic. The decomposition temperature can be adjusted by addition of activators (kickers). The most efficient activators are found to be transition metal compounds, amines, amides and glycols [16]. Popular examples are zinc-containing compounds such as zinc stearate, zinc oxide and zinc sulfide. But also calcium based oxides and salts can act as activators. These additives can decrease the decomposition temperature considerably, by as much as 40 °C by acting in an acid-base interaction [17]. Here, the transition metal of the kicking compound acts as a Lewis acid and can accept an electron from the Azo. Additionally, the formation of π-complexes can make the $-C-N=$ bond more susceptible to breaking due to a decrease in electron density between the nitrogen atoms [15].

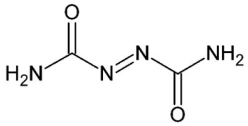

Figure 8: Chemical structure of Azodicarbonamide.

The expansion rate and ratio of a foam can be effectively determined by adjusting the amount of BA or the viscosity of the resin [18]. Blowing agents typically act as plasticizers in polymer melts, although little is known about the extent of this effect.

2.1.2.1 Azo decomposition kinetics

In order to properly control the foaming processing conditions it would be beneficial to also understand the decomposition kinetics of the employed blowing agent in combination with the added kickers. The experimental characterization of the decomposition kinetics of Azo are outside the scope of this work, but many studies on Azo decomposition are available as reference. Although some decomposition kinetics of Azo products have been published, the exact activation energies are not consistent for each product. The kinetics depend on the Azo particle size, as well as the heating rate, concentration and activator type and concentration. Although it is not straightforward to define the kinetics of the blowing agent used in this work based on published literature, there are some commonly observed trends.

As the decomposition reaction of Azo is autocatalytic, the decomposition occurs over a very narrow temperature range upon reaching the decomposition temperature. The kinetics are accelerated with higher temperatures and increased loadings of blowing agent. While the kinetics of decomposition are not affected by aging at increased temperature, the gas yield was observed to decrease upon aging [19]. This indicates that compounds should ideally not be kept at high temperatures. The decomposition temperature was indeed shown to decrease by addition of activators of different types [20]. This means that also the decomposition was accelerated with increased activator concentrations. While the exact rate constants and activation energy remain unknown for the employed Azo product, it is expected that Azo decomposition with sufficient amounts of activator would occur in readily at 180 °C.

2.2 Nucleation

Besides the type and concentration of the added blowing agent and other formulation-dependent effects, the foaming process can strongly influence the final foam morphology. Foaming typically consists of a series of several general events in which a gaseous compound or a volatile liquid is dissolved in the polymer melt at high pressure, creating a supersaturation. Nucleation of the system induces phase separation between the continuous phase and the gas, creating a situation of lower free energy [21]. Cells are formed in the continuous phase, creating a porous material [1, 22]. Cell growth consequently occurs through the diffusion of gas through the continuous phase to the nucleated cells. Bubbles continue to grow and coalesce, typically until an equilibrium is reached and the foam is stabilized or the bubble ruptures [23, 24]. Classical nucleation theory applies for the nucleation processes during foaming. Homogeneous and heterogeneous nucleation are distinguished.

2.2.1 **Homogeneous nucleation**

During homogeneous nucleation, bubble formation is induced simultaneously and randomly in the interior of a uniform material. This event is often prompted by a thermodynamic instability such as a change in pressure or temperature. The size of a nucleus defines the survival of the bubble, which can only grow spontaneously when the size exceeds the critical radius, which

corresponds with a free energy maximum [21]. The nucleation rate is strongly determined by the amount of gas, temperature, and magnitude of the pressure drop in the foaming experiment. During an injection process, one can thus make use of the pressure drop between the injection chamber and the mold to facilitate homogeneous nucleation. In traditional Crosslinked Injection Molding, homogeneous nucleation is induced by opening the mold at high velocity. An increase in the rate of the pressure drop has in literature been related to an increase in the nucleation density and thus the generation of a smaller cell size [25].

2.2.2 **Heterogeneous nucleation**

While homogeneous nucleation is mostly dependent on the processing conditions, heterogeneous nucleation is mostly promoted by specific additives in a material formulation. It is characterized by an increased probability of nucleation around the surface of foreign bodies, impurities, or phase boundaries where the activation energy for foaming is lower [21]. This drives the nucleation of bubbles on the interface of insoluble particles such as nucleating agents. In order to control the cell size and density of foams, nucleating agents are often incorporated in the formulation as additive. Examples of nucleating agents are: calcium carbonate, talc, sodium benzoate and stearic acid [2]. These additives can decrease the average cell size and promote the formation of a narrow cell size distribution.

2.3 Growth and Stability

Since the growth stage of a foam is out of equilibrium, it is metastable and thermodynamically inclined to collapse over time. The processes that act as a driving force towards the deformation of foams are: coalescence, coarsening and drainage, which all can ultimately lead to collapse of the foam [26]. The timescale on which these processes act can vary strongly, and the mechanism of collapse can be broken down in chemical and physical effects. The complex physics of foams distinguishes contributions from interfacial properties and properties of the bulk fluid [27, 28]. These contributions are sometimes governed by the familiar laws from colloid science. Events such as capillarity, surface elasticity and viscosity play important roles in the foam dynamics [29]. Although much empirical work is done, a good theoretical understanding of the physics of these processes is required in order to gain control over their manifestation.

2.3.1 **Drive towards collapse**

Pressure and pressure differences play a vital role in the formation and stability of all types of foams. Upon performing a foaming experiment, the gas pressure generated inside a gas bubble generated by the decomposition of a CBA or the facilitation of a PBA can lead to expansion of the material. The magnitude of this gas pressure, in combination with the nature of the polymeric system can determine the survival of such a foam structure; while this gas pressure is required to foam at all, it is also involved in many processes that can ultimately deflate the foam.

Coarsening and coalescence, events where two individual bubbles merge together to form a larger bubble with lower internal pressure are pressure driven. These effects lead to a decrease in number of droplets and increase in the average cell size. The force that counteracts these pressure differences is typically the surface tension of the material and the interplay of these forces determines the bubble's equilibrium shape. The surface tension drives the bubbles to reduce their

interfacial area, while the Laplace pressure drives bubble to grow, leading to lower internal pressures. The law of Laplace, which accounts for the pressure difference over a curved interface, captures this balance of forces. The Laplace (capillary) pressure for a spherical bubble is given by:

$$\Delta P = \frac{2\gamma}{r} \tag{1}$$

where ΔP is the pressure difference over the interface, γ is the surface tension and r describes the local radius of curvature of the interface.

In general, large droplets with relatively low internal pressure grow at the expense of small bubbles with high internal pressure. Because of these coarsening events, the total surface area is effectively reduced, which is in accordance with the drive towards thermodynamic equilibrium. The solubility of the gas in the fluid and the thickness of the cell walls strongly influence the extent of the coarsening behavior, making the choice of polymer essential in generating suitable cell size.

Pressure differences and gravity can also lead to the drainage of liquid from the lamella to the plateau borders, leading to thinning of the lamella and risking creation of open cells [29]. Flow of fluid through the channels between the bubbles as a result of local pressure differences and gravity is called drainage [30]. The pressure gradients, denoted as 'capillarity' cause fluid to drain from the thin films into the plateau borders (**Figure 9**) [31]. This so-called 'capillary suction' is caused by the lower pressure that is observed in the plateau borders than in the thin films. While gravity will initially also cause fluid to drain down from the lamella, capillary forces present themselves as competition against gravity. When evaluating the dynamic behavior of drainage in a foam, several contributing processes have to be taken into account. In addition to gravity: the viscous forces and capillary forces play the most significant role in drainage [32]. The rate of drainage has been described in many models but is difficult to catch in one universal equation. Although the contributions of gravity and capillary forces might be understood relatively well, the mobility of the liquid-gas interface is system dependent. These viscous forces contribute strongly to the displacement of the fluid in the porous system: they describe a fluid's resistance to flow. Since the viscosity of fluids can vary orders of magnitude and the surface viscosity can be different

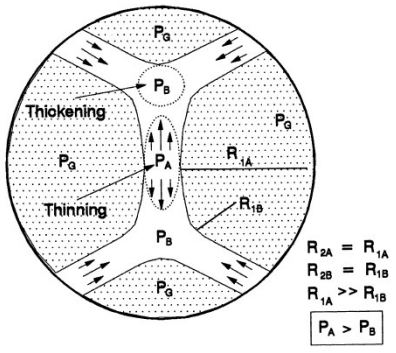

Figure 9: Pressure difference over the plateau borders, driving the flow of fluid towards the vertexes. (Schramm et al. 1994)

from the bulk viscosity [29], the contribution of these forces cannot always be effectively captured. Reynolds generalized the drainage rate of a liquid film between two, rigid surfaces. His result for the rate of drainage is given by [33]:

$$U = \frac{8h^3}{3\eta R^2}\Delta P \tag{2}$$

where h is half the thickness of the film, η the viscosity of the liquid, R the film radius and ΔP the capillary pressure. Although this relation may not be exact, and the conditions inside a foam may deviate from the made assumptions, this relation suggests the rate of drainage decreases with increasing viscosity of the fluid and increases with increasing surface tension. Stable foams should likely require high viscosities and low surface tensions, in order to retain small cell sizes. Depending on the chemistry of the polymeric phase and the temperature, the viscosity can vary orders of magnitude, and is thus a dominating factor in foam stability.

2.3.2 **Stabilization**

There are several ways to make use of the nature of a system to establish the required stability. While the addition of suitably interacting additives helps in foam stabilization for aqueous and polar systems, fluids with an inherently low surface tension cannot be stabilized analogously. Additives such as surfactants and surface active particles will thus neither be used nor described here. Although many polyolefinic systems might thus initially seem difficult to foam, one could make use of the rheological properties of certain (modified) polymers to create plastic foams.

Earlier described theory already confirmed the role of shear viscosity in foam stability. However, the mechanism of bubble growth mainly imposes extensional loads on the polymer as the polymer films are stretched during expansion. Many studies suggest a relation between the extensional properties of the bulk material and the foam structure. Insufficient extensional properties such as melt strength and lack of strain hardening could lead to rupture of the polymer films during blowing [34, 35]. Hence, this will lead to coalescence of the air pockets, undesired coarsening of the foam and a high open-cell content [36]. Strain hardening is present in molecular configurations that are unable to relax their stress faster than the timescale of the deformation. Examples of modifications that can be made to arrive at such properties are entanglements, crosslinks and long chain branching (**Figure 10**) [37]. Such chain configurations have finite extensibility due to their topological limitations but can sometimes also show stress-induced crystallization. This can contribute to an increased stress at high elongation. Such modifications

Figure 10: from left to right: entanglements, crosslinks, long chain branching.

also slightly decrease the crystallinity of the material which might promote the solubility and diffusivity of the gas through the polymeric phase [38].

2.4 Benchmark of midsole performance

Besides the obvious necessity of certain rheological properties for polymer resins in order to produce successfully stable foams, the degree of crosslinking also has an impact on the midsole performance. There is a range of requirements for optimal midsole performance, which are usually aimed towards providing sufficient cushioning (i.e. softening the force of impact during running) and lengthening the lifetime of the shoe. The requirements vary between different brand owners and are often tailored for specific shoe applications. Some of these foam properties are known to relate to the degree of vulcanization. This explains why upon developing a One to One Foaming method, a post-cure might be required if the mechanical properties of the foam dictate this.

2.4.1 **Density**

The degree of vulcanization is in context of Crosslinked Injection Molding often responsible for the density and optimal cell growth of the foam. A suitable density for athletic midsoles is usually around 0.2 g/cm^3, though densities between 0.15 – 0.35 g/cm^3 are observed depending on the shoe application and resin type. The density has also been shown to depend on the polymer crystallinity [39]. Besides the importance of the density, which also defines the weight of the shoe, several other properties will be listed here that have been shown to be important in midsole manufacturing.

2.4.2 **Hardness**

The hardness of a foam has been shown to be determined by the foam density. Low density foams yield corresponding low hardness, while foams with high density are generally hard [40]. There are several methods to determine the hardness of a material. Although parts of different scales such as Shore A and Asker C are overlapping, midsole foams are usually measured with Asker C. Asker C and Shore A are both non-destructive characterization tools that are pressed into a foam. The depth of an indenter is measured which provides a measure for the hardness. Midsole foams usually have a hardness between 45 and 60 on the Asker C scale. The comparison between the two scales are represented in **Figure 11**. The hardness plays a significant role in the comfort and dampening properties of the athletic shoe.

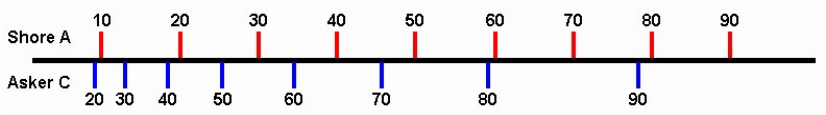

Figure 11: Overlap of the Shore A and Asker C scales for hardness.

2.4.3 **Compression set**

Compression set is an important property that determines the lifetime of the shoe; it defines the amount of unrecoverable deformation after the removal of a compression of a certain percentage and duration. The magnitude of this permanent set determines the capability of the foam to exhibit elastic recovery. INFUSE™ OBC is recognized by its good elastomeric properties, providing a lower compression set than EVA [41].

2.4.4 **Rebound resilience**

Rebound is a property that is especially relevant in athletic footwear applications. The rebound resilience is defined as the ratio of the energy that is returned after application of a deformation with a particular energy. The rebound resilience is an important measure for the cushioning effect in athletic midsoles and should be above 55%. The resilience has been related to the foam hardness, where the softest foams have the highest rebound [39].

2.4.5 **Split tear**

The split tear is the defined as the force that is required to split a foam along a slit in a rectangular test specimen. This property is very important for midsole durability, as it represent the resistance against cracking. Split tear typically requires a relatively densely crosslinked network. Also a high crystallinity has been related to improvement of the split tear, resulting from the prevention of crack propagation by the crystals [42]. The specification for split tear resistance is often desired to be above 2.5 N/mm.

2.4.6 **Cell size and distribution**

The cell size has been shown to contribute to the compression set of the material. Especially a decrease in cell size and cell wall thickness has been related to the reduction of the compressive strength of the material [43]. The exact consequence of the variation in cell size is unclear, but the majority of the foams for footwear applications are in the regime of 50-200 µm.

2.4.7 **Summary of desired properties for athletic midsoles**

An overview of the performance specifications for midsole foams are represented in **Table 1**.

Table 1: Performance requirements for midsole foams.

Property	**Typical requirement for footwear applications**
Density	0.15 – 0.3 g/cm^3
Hardness Asker C	45-60
Hardness Shore A	22-34
Compression set (50°C 50% compression)	<55%
Rebound resilience	>55%
Split tear	>2.5 N/mm
Cell size	<250 µm

3 Crosslinking chemistry

Upon crosslinking, individual polymer chains are irreversibly connected by chemical bonds. Crosslinked chains then become part of an insoluble network or 'gel' that can span through the entire sample. Such crosslinks are made by for instance: adding organic peroxides, silanes or applying high energy irradiation methods [44]. The degree of crosslinking can be controlled, leading to only fractions of a polymer to be part of the insoluble network. This fraction is often described as the 'gel content' (GC). The interconnection of the chains strongly affects the rheology of the polymer as compared to an entangled equivalent.

3.1 Peroxide modification

The most common method to introduce branching and crosslinking in a polyolefin system is by making use of peroxides. By mixing an organic peroxide in a polymer melt and subsequently heating above the decomposition temperature of the organic peroxide, radicals are created on a hydrocarbon backbone. Two radical backbones can recombine and thereby form crosslinks and long chain branching. One of the most commonly used peroxides, also in midsole manufacturing, is dicumyl peroxide [45] (**Figure 12**). The kinetics of cross-linking with DCP are strongly temperature dependent and vary with the amount of DCP added to the compound. Increasing amounts of added peroxide will generate a more densely crosslinked network [46]. Curing at high temperatures will result in full conversion in minutes, while low temperature curing can take hours.

In typical Crosslinked Injection Molding process where the use of chemical blowing agents is common, the rheological properties of the resin often suffer at the high processing temperatures that are required for CBA decomposition. At such high temperatures, the viscosity and melt-strength are typically insufficient to yield at a stable foam. This problem is usually solved by crosslinking prior to foam expansion. In the regime of under-curing, the cells typically rupture and deflate. On the other end of the spectrum, over-curing can result in improper expansion resulting at low expansion ratios. In One to One foaming with potential use of PBAs, the possibility to process at lower temperatures might reduce or eliminate the necessity of crosslinking prior to foaming [9].

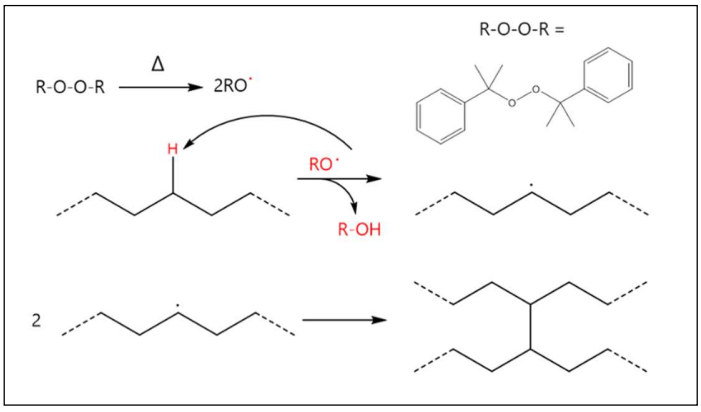

Figure 12: Crosslinking pathway of dicumylperoxide (represented on top right).

3.2 Silane crosslinking

An alternative method for crosslinking polyethylene-based polymers is silane crosslinking [47]. A silane compound that possesses at least one unsaturated bond can be chemically grafted onto any polyolefin in the presence of a radical generator, such as a peroxide. The other side groups of the silane compound should preferably be able to be split off by hydrolysis. For this, alkoxy residues are preferred. An example of a suitable molecule is vinyl trimethoxysilane (VTMS). Once grafted on the polymer chain, addition of water in will lead to the hydrolyzation of the alkoxy residues, leaving alcohol groups. This process can be accelerated in the presence of a (tin) catalyst. Two of these silanol groups can then form a siloxane by condensation, resulting in a crosslink [45] (**Figure 13**). Silane crosslinking can be a preferred crosslinking method because its initiation can be induced by water in the presence of a (tin) catalyst instead of elevated temperatures, although exposure to an oxidative environment at elevated temperatures (>190 °C) has also been proven to be effective [6].

Besides the siloxane crosslink that is generated in this procedure, it is inevitable that the peroxide will generate some direct crosslinks, though at a smaller rate. It has also been shown that silane grafting reduces the event of direct crosslinking [6]. G′ and G″ are lower in the presence of both VTMS and DCP than in the absence of DCP at the same concentration. The movement of the polymer chains to bring two radicals together is slower than the diffusion rate of the organosilane. Also chain scission will occur. Chain scission will lead to an unsaturation in the polymer chain, which can subsequently react with a radical chain to also form direct parallel crosslinks [6, 48].

In a One to One foaming process, it is hypothesized that silane curing can be used after foaming to provide the level of crosslinking to reach the anticipated performance. There have however been studies that suggest that crosslinking prior to foaming results in better properties than crosslinking after foaming.

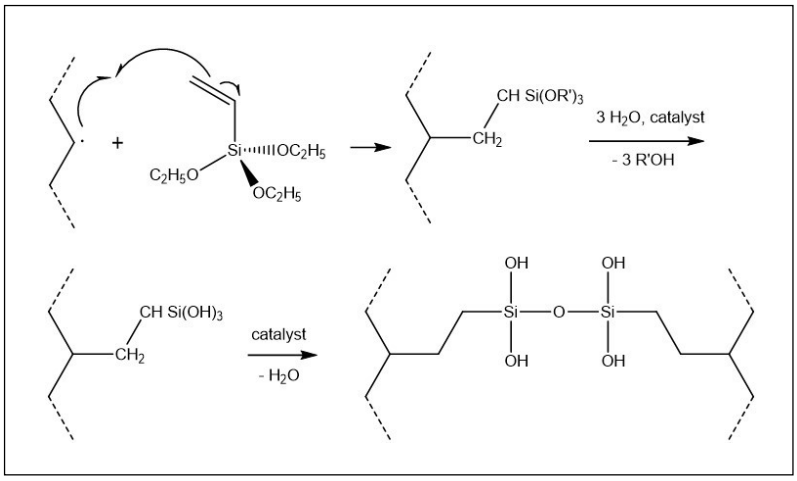

Figure 13: Grafting of trimethoxysilane to a polyethylene backbone, condensation then leads to the formation of a siloxane crosslink

4 Crosslinking kinetics

In order to elucidate the temperature dependent kinetics of dicumyl-peroxide modification of INFUSE™ OBC with different levels of peroxide modification, a rubber process analyzer (RPA) analysis was performed at three different temperatures (160, 180, 200 °C). Based on the RPA curing curves, the rate constant and activation energy of the curing process were determined. These parameters are used to predict the curing times that are required to reach 95% conversion at different temperatures and peroxide levels.

4.1 Theory

As described by Poongavalappil et al. [46] the kinetics of a crosslinking reaction with DCP can be captured in a first order reaction where the following equation is linear.

$$\ln(1 - X) = f(t) \tag{3}$$

Here, X is the conversion ratio which is calculated from

$$X = G'(t)/G'_{max} \tag{4}$$

Equation 3 originates from the conventional reaction kinetics equation:

$$\frac{dX}{dt} = K^{(n)}\,(1 - X)^n \tag{5}$$

Where dX/dt describes the rate of the reaction, and K is the rate constant. n describes the order of the reaction, which is set to 1 in this context. Arrhenius' law can be used to describe the temperature dependence of the reaction rate as:

$$K = A.\,e^{-\frac{E_A}{RT}} \tag{6}$$

and

$$lnK = lnA - \frac{E_A}{RT} \tag{7}$$

E_A is the activation energy in J mol^{-1}, R is the gas constant, 8.314 J mol^{-1} K^{-1}, T is the temperature in K and A is the pre-exponential factor. The rate constant can be found at different temperatures by determining the slope of **Equation 3**. The activation energy and pre-exponential factor can subsequently be found by linear regression of **Equation 7**.

4.2 Experimental characterization of peroxide curing kinetics

4.2.1 **Materials and Methods**

All polymers used in this work were provided by the Dow Chemical Company. INFUSE™ OBC was chosen due to its expected advantageous performance in footwear applications. Two polymers with different melt indices (MIs) with the same density were selected. In this work, there will be often referred to the Melt Index (MI) or Melt Flow Index (MFI) of a resin grade. This is a parameter that is typically defined for thermoplastic materials to describe their tendency to flow in the molten state. The MI describes how much weight of a molten polymer is able to flow in ten minutes through a capillary of fixed length and diameter at fixed temperature and pressure. The grades of INFUSE™ OBC products have a well-defined MI between 0.5 and 15 g/10 min (2.16 kg @ 190 °C). In general, a high MI corresponds to a low viscosity, and typically a relatively low molecular weight with respect to low MI grades with high viscosity. Elastomers with a MI of 1 and 5 should provide suitable processability in injection methods for footwear applications.

The used Dicumyl peroxide (DCP) powder masterbatch was Luperox DC40P-SP2 delivered by Arkema. The concentration of active peroxide was 40% blended in an inert filler, scorch protected to allow for high temperature processing. Scorch is the event of premature curing during processing at high temperatures. Scorch protection is required for processing of INFUSE™ due to the relatively high melting point (**Table 2**) as a result of the large crystalline blocks. The half-life $t_{1/2}$ of this peroxide is 1h at 137 °C. The three polymers were compounded for the following concentrations of active DCP: 0, 0.2, 0.4, 0.6, 0.8, 1 and 1.2 parts per hundred resin by weight (phr). These concentrations were in the range between unmodified resin and concentrations found in typical footwear formulations [20]. OBC and peroxide were mixed on a Colin roll mill with the front roll at 130 °C and the back roll at 125 °C and a rotation speed of 8 rounds per minute (rpm).

The crosslinking kinetics were investigated on a Rubber Process Analyzer, RPA-2000 from Alpha Technologies. The polymers with the different loadings of peroxide were analyzed at 160, 180 and 200 °C for 1.5 h, 15 min and 7 min respectively. RPA measurements were performed at an angle of 0.5° which was determined to be in the linear viscoelastic regime of the highest crosslinked sample. A frequency of 10 rad/s (=1.667 Hz) was employed. Samples were placed in between two polystyrene films, which were observed not to affect the measured properties.

Table 2: properties of OBCs used in this work

	Density (g/cm^3)	MI (g/10 min 190 °C/2.16 kg)	T_m (°C)
INFUSE™ 9100	0.877	1	120
INFUSE™ 9500	0.877	5	122

4.2.2 **Experimental results**

A typical development of mechanical properties at 180 °C is shown in **Figure 15.** Analogous data for different temperatures and MI is represented in **Appendix A**. In line with the expectations, the pure polymer does not show an increase in storage modulus over time. All peroxide treated samples showed in increase in storage modulus, reaching a plateau at approximately 2, 9 and 60

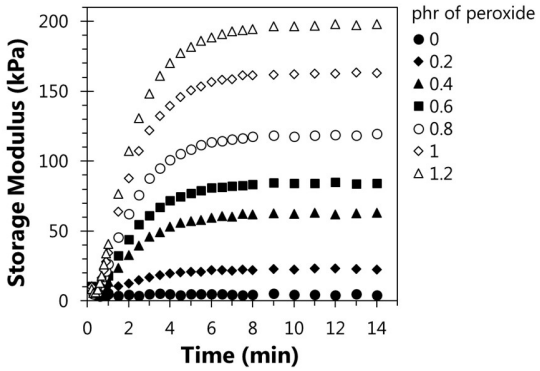

Figure 15: Curing curve of INFUSE™ 9500 at 180 °C measured at 10 rad/s.

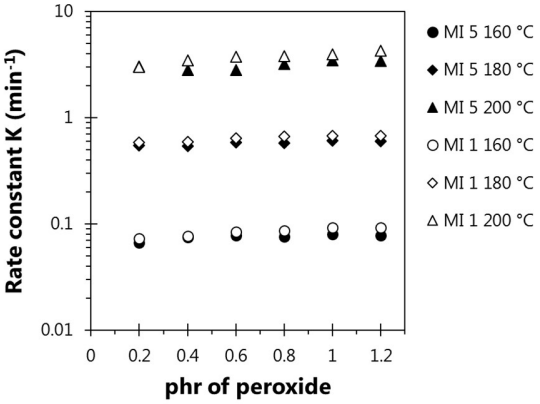

Figure 14: Rate constants determined for INFUSE™ 9500 and INFUSE™ 9100 at different temperatures and peroxide levels

minutes for 160, 180 and 200 °C respectively. For these time scans for different MI, temperature and peroxide loading, the conversion ratio was calculated using **Equation 4** such that G'_{max} corresponds to a full conversion of 1.0 (100%), which is defined as the average equilibrium G'.

The rate constants were determined by fitting the slope of **Equation 3** for the different peroxide levels at different temperatures. The linear nature of this relation is in agreement with the prediction of the applicability of first order reaction kinetics. The rate constants, as depicted in **Figure 14** are strongly temperature dependent, but much less so on the peroxide loading and polymer melt index. The curing rate can thus be accelerated significantly by increasing the temperature, irrespective of the peroxide concentration.

The activation energies and pre-exponential factors were determined for both OBC materials by linear regression of **Equation 7**. Results are shown in **Figure 16** and average values are reported in **Table 3** Unlike the results from Poongavalappil et al. [46] our determined activation energy is approximately equal for the different levels of peroxide. The found activation energies are consistent for both melt indices of INFUSE™ OBC.

Table 3: Average rate constants, activation energy and pre-exponential factor for INFUSE™ 9500 and 9100

MI of INFUSE™ OBC	Average rate constant K (min^{-1}) at temperature (°C)			Activation energy ($kJ\ mol^{-1}$)	Frequency factor A
	160	**180**	**200**		
5	0.075	0.58	3.1	159	41.5
1	0.084	0.64	3.7	161	42.2
Average	0.080	0.61	3.4	160	41.9

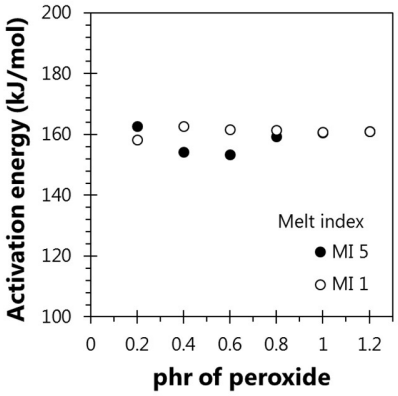

Figure 16: Activation energy of INFUSE™ 9100 and 9500 as a function of peroxide level.

4.3 Empirical model for peroxide curing

Since the activation energy and pre-exponential factors are approximately constant for the probed melt indices and peroxide concentrations, the average values were used to predict the rate constants at a range of temperatures via **Equation 6**. Results are represented in **Figure 17**. With these rate constants, the time that is required to reach 95% conversion is calculated by:

$$t_{95} = \frac{\ln(0.05)}{-K} \tag{8}$$

The times that are required for 95% conversion as a function of the temperature are shown in **Figure 17**. Crosslinked Injection Molding typically occurs at a mold temperature of 180 °C. Based on this kinetics study, the material should be heated for at least 5.4 minutes to achieve a conversion of 95%. Evidently, when using chemical blowing agents the curing kinetics and blowing agent decomposition kinetics should both be accounted for when choosing processing conditions.

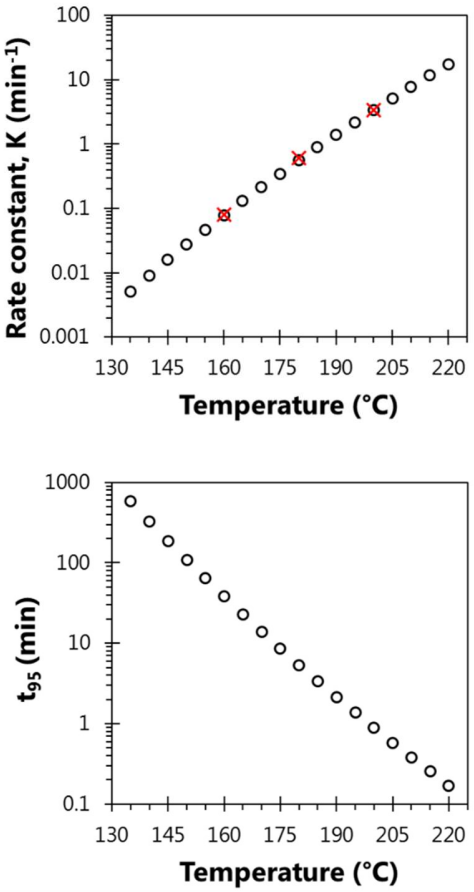

Figure 17: Top: calculated rate constants for peroxide curing of INFUSE™ OBC at different temperatures. Experimentally determined rate constants are represented in red. Bottom: Conversion times as a function of temperature.

5 Rheology

One of the objectives of this work is to relate the rheological properties of a peroxide modified formulation to the foam morphology and structure for the conventional and novel foaming process. These properties, in combination with the mechanical properties will be used to define a processing window for INFUSE™ OBC. Both the effect of the shear rheology and extensional properties are of interest. The shear rheology mostly plays a role during injection procedures: in Crosslinked Injection Molding the curing occurs after injection, so the peroxide loading thus does not affect the ability to inject. In One to One Foaming is expected that small levels of crosslinking would provide the properties needed for the formation of a stable foam, while remaining plastic enough to be injected. The foam stability will be mostly related to the extensional behavior of the formulation.

5.1 Shear rheology

To analyze the effect of peroxide modification on the flow behavior of peroxide modified OBC, the shear rheology is characterized. These data will be used to interpret the elongation behavior of a material during foaming, but also to evaluate the behavior during processes of high shear such as injection molding and extrusion.

5.1.1 **Theory**

A deformation in simple shear is represented by a material being deformed by two parallel surfaces. While solids behave purely Hookean, and liquids purely Newtonian, polymer melts are viscoelastic. In practice, this means that they display a combination of liquid and solid behavior depending on the magnitude and duration of an applied stress. Modern technology allows for easy characterization of rheological behavior in a linear viscoelastic measurement in oscillatory shear on a conventional 'rheometer'. In a typical controlled strain rheology measurement, a sinusoidal strain of angular frequency ω is applied to a sample between two parallel plates as:

$$\gamma(t) = \gamma_o \sin(\omega t) \tag{9}$$

A suitable amplitude of the oscillation should be found by performing an amplitude sweep to define the range of the linear viscoelastic regime of the material. At low strains, the stress and the strain are proportional. The viscoelastic response of a material at different timescales (1/ω) can then be easily extracted by measuring at different angular frequencies in a 'frequency sweep'. A viscoelastic response can be divided in a purely elastic response, where the stress is perfectly in phase with the strain:

$$\sigma(t) = G\gamma(t) = G\gamma_0 \sin(\omega t) \tag{10}$$

and a purely viscous response, where the stress is out of phase, with a phase angle δ=π/2, with the deformation

$$\sigma(t) = \eta \frac{d\gamma(t)}{dt} = \eta\gamma_0\omega \cos(\omega t) = \eta\gamma_0\omega \sin\left(\omega t + \frac{\pi}{2}\right) \quad (11)$$

For a viscoelastic material, the linear response can be generalized as [49]

$$\sigma(t) = \sigma_0 \sin(\omega t + \delta) \quad (12)$$

The stress can thus be captured in an in-phase and an out-of-phase function through

$$\sin(\omega t + \delta) = \cos(\delta)\sin(\omega t) + \sin(\delta)\cos(\omega t) \quad (13)$$

as

$$\sigma(t) = \gamma_0[G'(\omega)\sin(\omega t) + G''(\omega)\cos(\omega t)] \quad (14)$$

where

$$G' = \frac{\sigma_0}{\gamma_0} cos\delta \quad (15)$$

and

$$G'' = \frac{\sigma_0}{\gamma_0} sin\delta \quad (16)$$

Here G' is defined as the storage modulus, and G'' as the loss modulus, where G' corresponds to the in-phase 'elastic' response, representing the storage of energy in the material which is again released when the deformation is removed. G'' represents the out-of-phase 'viscous' response, this is a measure for the energy that is dissipated during the deformation. The balance between these moduli represents the elasticity of the material in the loss tangent.

$$tan\delta = \frac{G''}{G'} \quad (17)$$

During an oscillatory rheology experiment, Newton's law still applies, resulting in a description for the complex viscosity [50]

$$\eta^* = \sigma(t)/\dot{\gamma}(t) \quad (18)$$

The equilibrium configuration of a linear polymer is an entangled coil. Upon applying a shear deformation to such a coil, the entangled coils relax and orient themselves in the direction of the shear deformation. Consequently, the resistance to flow reduces and the viscosity reduces accordingly. This presents itself as shear-thinning behavior with increasing shear rates. At high shear rates when maximum orientation is achieved the viscosity will not reduce further. The typical shape of a shear complex viscosity curve as a function of the frequency is represented in **Figure 18**.

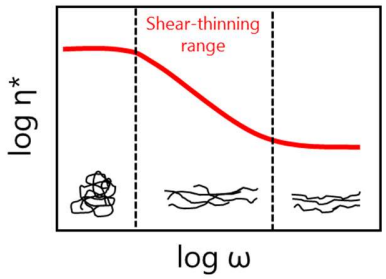

Figure 18: Shear viscosity of linear polymers as a function of the shear rate. The behavior consists of three regimes: the first Newtonian regime, the shear thinning regime and the second Newtonian regime.

Upon significant modification with crosslinking agents the shear rheology becomes notably different. While uncrosslinked chains can move freely, crosslinked chains are not able to undergo macro-Brownian motion [51]. This prevents the crosslinked polymer from melting and flowing when the temperature is increased, leading to an observation of a rubbery plateau, where the changes in viscosity and modulus are relatively small up to temperatures where the polymer degrades (**Figure 19** left). The gel content also affects the viscoelastic properties as function of shear rate; lightly crosslinked polymers (with low GC) behave similarly to uncrosslinked equivalents and behave as represented in **Figure 18**. With increasing GC the behavior converges to a situation where a first Newtonian regime is absent (**Figure 19** right).

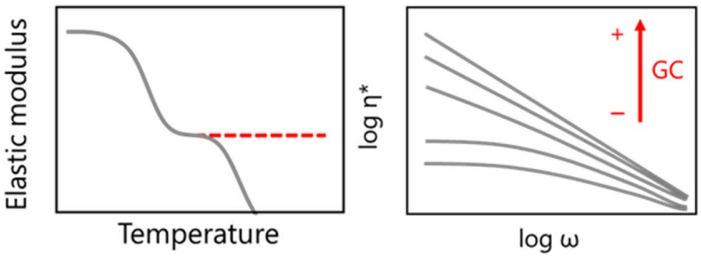

Figure 19: Left: temperature dependence of the elastic modulus for crosslinked (red) and uncrosslinked (grey) materials. Right: effect of gel content on complex viscosity.

In 1958, an empirical relation between the steady shear viscosity as a function of the shear rate and the complex viscosity as a function of the frequency was introduced [50]. This relation is called the Cox-Merz rule and follows:

$$\eta(\dot{\gamma}) = |\eta^*(\omega)| \tag{19}$$

This relation holds for molten polymers tested in the linear viscoelastic regime, but has also been shown to be valid for crosslinked polymers [52].

5.1.1.1 Time temperature superposition principle

For polymer melts, there is a correspondence between time and temperature, which is defined as the 'time-temperature superposition principle'. Besides the obvious relation to the strain rate, the viscosity is also strongly temperature dependent as heating leads to softening of the polymer. The same relaxation state can thus be achieved at high temperature and low-shear conditions, or low temperature and high-shear conditions. The temperature dependence is normally described in an Arrhenius-type equation:

$$\eta = Ae^{E_A/RT} \tag{20}$$

Where E_A is the activation energy of flow, R the gas constant and T the temperature. The activation energy represents here the energy that is required to exceed the energy barrier related to flow. This relation is generally applicable for polymer melts. The effect of temperature can typically be described by a shift factor, where an oscillatory function can be shifted with respect to a reference temperature.

$$a_T = \eta(T)/\eta(T_{ref}) \tag{21}$$

According to the Arrhenius law, the following holds for the shift factor:

$$a_T = \exp\left(\frac{E_A}{R}\left(\frac{1}{T} - \frac{1}{T_{ref}}\right)\right) \tag{22}$$

5.1.2 **Methods**

Compounded material with different loadings of peroxide (see **paragraph 4.2.1**) were compression molded and cured in a Lab Tech Press LP-S-80. Stacks of roll milled compound were preheated inside the molding press for 2 minutes at 180 °C at 10 bar, and consequently fully pressed at 120 bar for 8 minutes to a thickness of 2 mm to ensure complete crosslinking, which was determined in **Chapter 4** to take approximately 5 minutes. After complete pressing and curing, the samples were gradually cooled inside the press to 40 °C before removing from the molding plates to ensure proper relaxation of the chains.

At least 24 hours after compression molding, disks with a diameter of 8 mm were punched from the cured sheets with a cutting die. Shear rheology was measured in a TA instruments HR-2 rheometer with temperature chamber cooled with nitrogen. All samples were first subjected to a strain amplitude sweep experiment at 25 °C at an angular frequency of 10 rad/s from 0.01 to 10% to determine the location of the linear viscoelastic regime. Based on that information, a suitable strain amplitude was chosen to perform the frequency sweeps. As samples without or with low levels of peroxide have a relatively low viscosity, the 8 mm parallel plate geometry was

unsatisfactory in receiving the required signal. The resolution could be improved by using a larger geometry plate (25 mm) to reach a higher torque.

Frequency sweeps were then measured at, 130, 150 and 180 °C to correspond with the temperatures of the extensional rheology experiments as reported in **paragraph 5.2.** Frequency sweeps were taken as a logarithmic sweep between 100 and 0.1 rad/s, this means that the datapoints were recorded with equal spacing on a logarithmic scale.

5.1.3 **Results and discussion**

An example of the frequency dependence of the complex viscosity of INFUSE™ 9500 at 130°C at different peroxide concentration is shown in **Figure 20**. As discussed in earlier in this chapter, the rheological behavior can undergo dramatic changes upon modification with peroxide. The shape of the curve of the pure polymer is in agreement with the typical behavior of polymer melts. At low frequencies, there is a clearly defined first Newtonian regime, followed by a shear-thinning regime at higher frequencies. With increasing peroxide levels, which are expected to yield increased gel levels, the rheological behavior starts showing more significant deviations from melt-behavior. Here the presence of a first Newtonian regime seems to vanish in the probed frequency range, especially from 0.6 phr of peroxide upwards. Due to this notable change in behavior, samples with 0.04 and 0.1 phr of peroxide were added to the analysis to analyze this crossover regime in more detail.

By modifying the polymer with relatively increasing fractions of crosslinking agent, the complex viscosity of INFUSE™ OBC could be transformed by orders of magnitude from 10^3 to 10^6 at small angular frequency. This shows the power and tunability of crosslinking processes in polymer engineering. The trends of the complex viscosity at different peroxide levels as represented above is similar at all measured temperatures and both melt indices (see **Appendix B**). It is noteworthy that the temperature affects the magnitude of the complex viscosity exclusively for formulations with peroxide levels below approximately 0.2 phr of peroxide. A comparison of the temperature dependent behavior for two different loadings of peroxide (0.1 phr and 1 phr) for INFUSE™ 9500 is shown in **Figure 21**. The complex viscosity of INFUSE™ OBC modified with 0.1 phr dicumyl peroxide clearly shows a shift with temperature, in line with the behavior of polymer melts. During the experiments it was also observed that samples with this type of temperature dependence

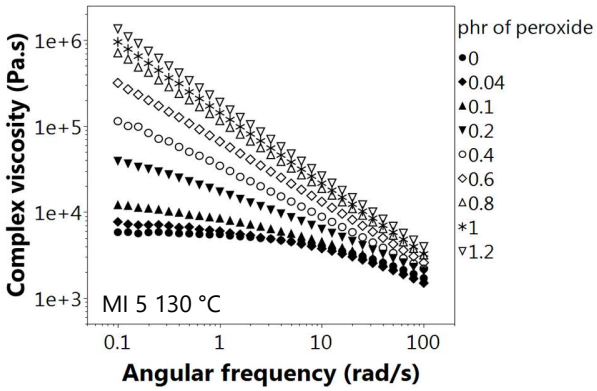

Figure 20: Frequency dependence of the complex viscosity of INFUSE™ 9500 at 130 °C.

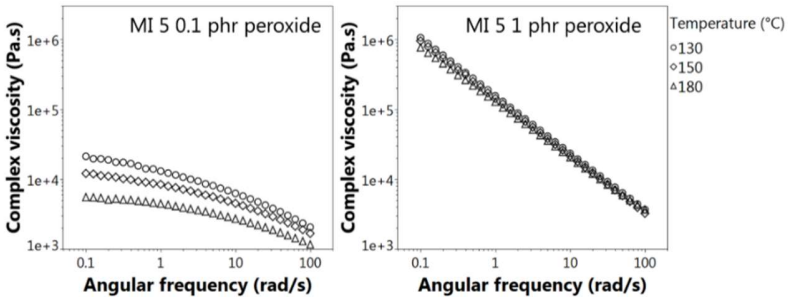

Figure 21: The frequency dependent complex viscosity η* of INFUSE 9500 modified with 0.1 and 1 phr of dicumyl peroxide represented at 130, 150 and 180 °C.

were clearly molten. On the other hand, samples with higher peroxide concentrations (>0.2 phr) showed an independence to the temperature and also kept their shape upon heating. This behavior is more in line with crosslinked 'rubbery' behavior, as these types of materials typically show a rubbery plateau above the melting temperature of the polymer.

An overview of the behavior of the complex viscosity at ω=0.1 rad/s is represented in **Figure 22**. It becomes immediately apparent that for both MIs an increase in complex viscosity is observed with increasing peroxide modification. The relatively high starting viscosity of the material with the lower melt index results in an effective vertical shift with respect to the melt index. The temperature dependence of the complex viscosity is especially apparent in the thermoplastic regime. The shear complex viscosity is not typically regarded as a representative description for the rheology during a foaming process, which are dominated by extensional deformations. In some cases however, the trends in the shear viscosity are in agreement with the trends in the uniaxial extensional viscosity, this will be verified later in this chapter.

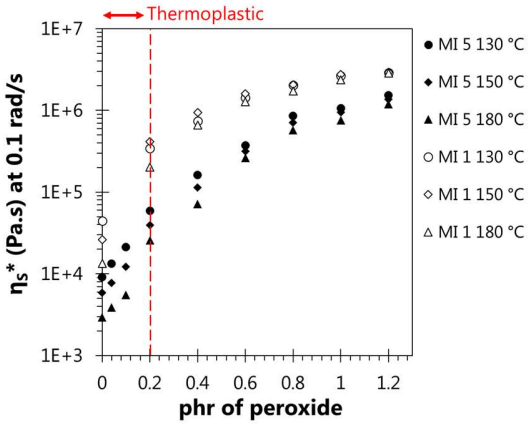

Figure 22: Overview of the complex viscosity measured at 0.1 rad/s for INFUSE™ 9500 and 9100 at different temperatures as a function of the peroxide level.

Although the experimental detection of the gel levels is outside the scope of this work due to the limited access and experimental challenges of solvent extraction methods, an estimation of the gel point can be extracted from oscillatory shear rheology characterization as described by Gendron et al. [53] The values for tanδ are typically are a good description of the elasticity of a polymer. The gel point has been shown to correspond to an independence of tanδ to the frequency in a shear rheology experiment plotted on logarithmic axes, so

$$\frac{d\log(tan\delta)}{d\log(\omega)} = 0 \tag{23}$$

When this is the case, G' and G" are parallel on the conventionally used logarithmic axes as a function of the frequency. For the two melt index materials, the slope as described in **Equation 23** was determined at frequencies between 10 and 100 rad/s at 130 °C by fitting a power law function though the data for tanδ as shown in **Appendix B**, the same trends were verified for the other temperatures. Results of this analysis are shown in **Figure 23**. An indication for the gel level was found by a normalization of the slopes to the condition that the pure resin corresponds to a gel fraction of 0. The gel curves as a result of DCP modification as presented here are similar to the results found by Poongavalappil et al. based on solvent extraction methods of DCP modified ENGAGE™ POE [46]. Both melt index materials converge to the gel point with increasing peroxide modification. The OBC with MI=1 appears to reach the gel point a bit sooner than the OBC with MI=5. In practice, only samples modified with concentrations below 0.2 phr showed thermoplastic behavior at elevated temperatures, these samples are in **Figure 23** represented in red.

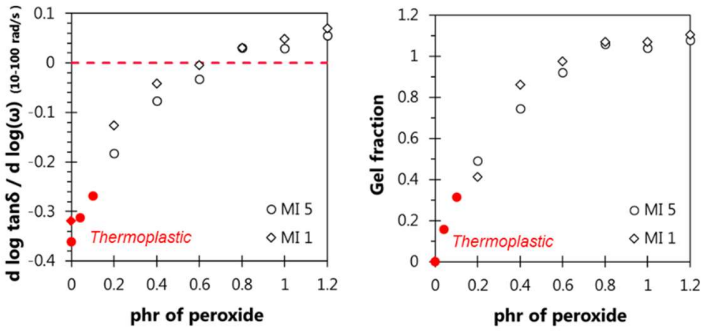

Figure 23: Left: The derivative of the loss tangent with respect to the frequency between 10 and 100 rad/s as a function of the peroxide loading for INFUSE™ 9500 and 9100. Data from oscillatory rheology measurements at 130 °C was used. Right: normalization to the gel fraction.

5.1.4 Time temperature superposition

For thermoplastic samples that show a clear temperature dependence, we hypothesized the applicability of the time temperature superposition principle and the Cox-Merz rule (**Equation 19**) to define the activation energy for flow at different peroxide levels. A verification of the applicability of the superposition principle was performed by plotting the phase angle (°) as a function of the complex modulus G*. When these functions overlay at each temperature, the calculation of 1D shift parameters should suffice in yielding an activation energy of flow which

can consequently be used to predict the viscosity at chosen peroxide levels and temperatures. The following steps were taken for INFUSE™ 9500 with 0, 0.04 and 0.1 phr of peroxide. The Excel solver was used to determine the Cross model parameters at the reference temperature. Here 130 °C was consistently used as reference temperature. The Cross model is defined as:

$$\eta = \frac{a_T}{b_T} c_1 / (1 + (c_3 * a_T * \dot{\gamma})^{c_2}) \tag{24}$$

As the density dependence of INFUSE™ OBC on the temperature was not known, the vertical shift factor b_T was set as 1. For the different temperatures, the horizontal shift factors a_T were determined again with the Excel solver. These shift factors yield the activation energy of flow E_a via **Equation 22**.

The best fits were obtained for the pure polymer, but acceptable fits were obtained for the slightly modified samples. The found Cross model parameters and activation energies were fitted to the levels of peroxide. This resulted in a tool that is able to approximate the viscosity at any shear rate and temperature of choice for any peroxide concentration between 0 and 0.1 phr of peroxide. The variation of the Cross parameters with peroxide content is represented in **Figure 24**.

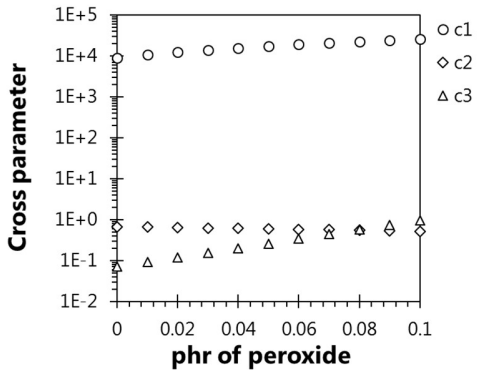

Figure 24: variation of the Cross parameters with peroxide concentration.

The results for a range of simulated peroxides concentrations are shown in **Figure 25,** in which was assumed that the Cox-Merz rule holds. This figure supports the notion that fits based on the time-temperature superposition principle perform best for unmodified samples. It seems the model overestimates the viscosity slightly for peroxide modified samples. For the purpose of approximating the order of magnitude of the viscosity at different temperatures, peroxide levels and shear rates this model suffices. Due to the lack of data in the thermoplastic regime it was not possible to make a similar tool for INFUSE™ 9100, although this could still be of interest for the ability to make predictions in the context of a foaming window. A tool like this can be efficiently used to predict the viscosity of a given formulation in the thermoplastic regime, without the necessity of sample preparation and experimental efforts.

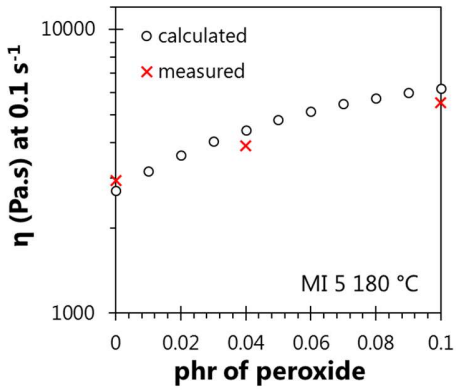

Figure 25: Calculated viscosities for INFUSE™ 9500 at 0.1 s^{-1} and 180 °C for different simulated levels of peroxide. The experimentally determined values were plotted in red.

5.2 Uniaxial extensional rheology

Three general modes of extensional flow are distinguished: uniaxial, planar and biaxial extension. In foaming, the main mode of extension is biaxial as bubble expansion occurs in three dimensions. The scarce amount of available studies on extensional properties describe mainly uniaxial extension due to the experimental challenge associated with biaxial extension methods. Biaxial, as well as uniaxial extension equipment are often unavailable in laboratories and experiments are often challenging.

5.2.1 **Theory**

The most common method to analyze the extensional properties of a polymer (melt) is uniaxial extensional rheology. These experiments are typically conducted in a nitrogen filled chamber at elevated temperatures above the melting point of the polymer melt [35]. Here, a rectangular test specimen is elongated from an initial length L_0 to a final length L at a fixed extensional rate [54]:

$$\dot{\varepsilon} = \frac{1}{L}\frac{dL}{dt} \tag{25}$$

If a test specimen is elongated at this rate for a time t to a length L, the true strain or Hencky strain is then defined as

$$\varepsilon = \dot{\varepsilon}\, t = \ln\left(\frac{L}{L_0}\right) \tag{26}$$

While the stress is

$$\sigma_E = \frac{F}{A} = \dot{\varepsilon}\, \eta_E{}^{+}(t) \tag{27}$$

The extensional viscosity $\eta_E{}^{+}$ is sometimes also called the 'uniaxial stress growth coefficient' because as the stress increases with time, $\eta_E{}^{+}$ is also increasing with increasing deformation. In a typical foaming process, the acting strain rate is approximately 1 s^{-1} and the Hencky strains are between 3 and 4 [36].

Figure 26: Example of uniaxial extensional measurement rheology tool for a rotational rheometer.

The extensional viscosity is nowadays typically measured on a rotational rheometer equipped with an extension tool for elongational viscosity. Such tools typically are built from two oppositely rotating drums onto which a rectangular sample can be fixed (**Figure 26**). Such tools are only suitable for melts with a sufficiently high viscosity, as otherwise there is a risk of sample sagging.

Depending on the nature of the polymeric system, the response to such an extension can vary. For Newtonian fluids and linear polymers, the extensional viscosity is three times larger than the shear viscosity. This behavior is also captured in Trouton's law [36]:

$$\eta_E{}^+ = 3\eta_s{}^* \tag{28}$$

However, dynamics of bubble growth become much more complex for materials that are strongly dimensionally constrained. Such materials exhibit strain hardening behavior, sometimes called extensional thickening. This effect results in a deviation from the Trouton ratio, leading to an increased viscosity at large strain. The magnitude of strain hardening, or strain hardening index (SHI), is often characterized as the ratio between the observed extensional viscosity at a particular time and strain rate, and an artificial extensional viscosity in the linear viscoelastic regime at the same time (represented as the grey line in **Figure 27**) [35, 36]. This artificial extensional viscosity is typically found by using the complex viscosity curve from a frequency sweep in oscillatory shear (applying Trouton's law as represented in **Equation 28)** or by fitting the linear viscoelastic regime of the extensional viscosity curves. Here we utilize the former method which is defined as:

$$SHI = \eta_E{}^+(t)/(3\eta_s{}^*(at\ \omega = 1/t)) \tag{29}$$

5.2.2 **Rheology modification and foaming**

The generation of strain hardening behavior is generally related to the physical restriction of polymer mobility. Short chain, linear polymers are usually difficult to foam, as they have insufficient strain hardening behavior. During expansion, the cell walls of such linear polymers become very thin, and ultimately break. Although an increase in molecular weight does not necessarily generate strain hardening behavior, the extensional viscosity increases in line with the effect on the shear viscosity following the Trouton rule. On the other hand, parameters like the molecular weight distribution (MWD) can generate strain hardening behavior. Blending a linear polymer with a small fraction of a high molecular weight (miscible) polymer can cause deviations from the Trouton ratio [55]. Blends with these bimodal molecular weight distributions can exhibit strain hardening behavior and are sometimes called 'High melt strength polymers' [56].

Improvement of the elasticity and strain hardening behavior can also be achieved by modifying linear polymers by introducing long chain branching (LCB) and crosslinks [23, 35, 57]. The enhancement of strain hardening behavior is resulting from constrained chain relaxation. Gotsis

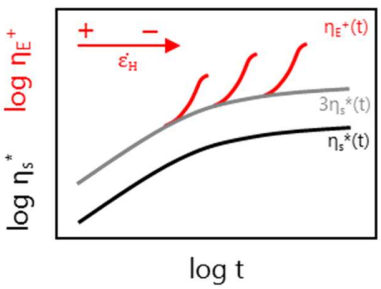

Figure 27: Representation of the relation between the shear viscosity and the extensional viscosity

et al. showed that both the melt strength and strain hardening index of a polymeric system increase with larger branching number, provided by different (small) loadings of peroxide [57]. Linear polypropylene was shown to lack strain hardening behavior and performed poorly in foam processing. By increasing the entanglement density in the melt by peroxide modification, strain hardening behavior was enhanced. Because of the improved extensional properties, foam quality was also improved with respect to the linear PP. The same was shown by Laguna-Gutierrez et al. for HDPE and PP modified with organic peroxides. [37, 58] Lack of strain hardening was shown to result in high open cell content, but by increasing the fraction of High Melt Strength (HMS) PP the cell size and open cell content decreased accordingly. Mixing of linear polymers with moderate amounts of branched polymer may also lead to desirable melt properties. Spitael et al. studied foam densities created by water blowing of polypropylene mixed with different ratios of a branched polypropylene [59, 60]. Branched polymers on their own showed strain hardening behavior, while linear polymers did not. Blending of linear polypropylene with a moderate amount (25%) of branched PP resulted in strain hardening behavior and a decrease of the foam density and a smoother foam surface. Blends with 50% branched PP showed higher foam densities and yielded poor foam quality.

Although a systematic study is lacking in literature, these findings suggest the presence of an optimum in strain hardening in relation to foam quality, where excessive strain hardening would impair the mechanical properties, such as strain at break, required to obtain satisfactory foaming behavior [57]. In this work, the extensional properties of the polymeric system will be related to the foamability, foam morphology and foam performance.

5.2.3 **Methods**

In order to find a description for the extensional properties that are relevant in foaming processes, the uniaxial extensional rheology was measured at different temperatures. Trends in the extensional behavior were extracted from relevant strain rates and Hencky strains. This also includes calculation of the strain hardening index SHI.

The same compounds as described in **paragraph 4.2.1** were here used for uniaxial extensional rheology characterization. Square plates with a thickness of 0.5 mm were compression molded and cured in a Lab Tech Press LP-S-80. The compounds were compressed in a Teflon coated mold using the following layers: press plate, aluminum plate, aluminum foil, Teflon coated mold with sample, aluminum foil, aluminum plate, press plate. Sheets were preheated at 180 °C for 180 s at 10 bar, followed by a full compression for 360 s at 120 bar. The sheets were cooled at a constant cooling rate to 40 °C to ensure full relaxation of the chains.

For the uniaxial extensional rheology experiments, rectangular test specimen with dimensions 13x12.7 mm were cut out from the cured sheet with a cutting die. Dimensions were also measured for each individual sample with a caliper tool and fed into the rheometer software for each individual measurement. The experiments were performed on an Anton Paar MCR 702 with a Convection Temperature Control Device (CTD) 450 oven attached with a Universal Extensional Fixture (UXF) tool. The measurements were performed at three different extensional strain rates (0.1, 1 and 10 s^{-1}) at three different temperatures (130, 150 and 180 °C). Prior to the test procedure, a pre-stretch was performed at the corresponding strain rate. Data-points were recorded at

logarithmically spaced time intervals. At each of these intervals with corresponding Hencky strains, this yields a measure for the extensional stress and the extensional viscosity.

5.2.4 **Results and discussion**

UXF measurements are typically conducted for polymer melts that have sufficient extensional behavior to not show any sagging upon fixation to the measurement tool. Since the pure polymer melts of INFUSE™ 9500 showed too much sagging, these measurements were excluded from this report as no reproducible data was recorded. Since in the range of the measured samples here only the pure resins showed thermoplasticity, other crosslinked samples could not be molten onto the UXF drums. Stitches were used to fix these test specimen to the measurement tool. Samples that were crosslinked so far as to retain high stiffness even upon heating often slipped from the drums during the measurement, this was the case for INFUSE™ OBC 9100 modified with 1.2 phr of peroxide. For this reason, this data was also excluded from this study. No modified samples between 0 and 0.2 phr of peroxide were included in this analysis. Understanding the extensional behavior for more formulation in the thermoplastic regime could however be of interest in later studies in relation to One to One foaming applications.

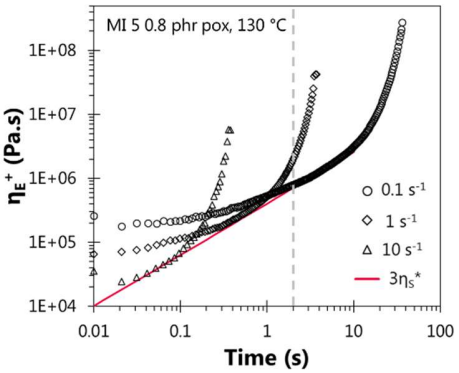

Figure 28: Extensional rheology of INFUSE™ 9500 modified with 0.8 phr peroxide at 130 °C. The linear viscoelastic regime is plotted as $3\eta_S^*$ represented in red. The grey dashed line indicates ε=2

Uniaxial extension of elastomeric materials not showing thermoplasticity might not have the same significance as that of polymer melts. In crosslinked samples, the retractive force is dominating in the behavior, meaning that the extensional viscosity for crosslinked samples is physically different than that of thermoplastic resins. Nevertheless, the extensional behavior can still be of relevance for the detection of the processing window. Strain hardening behavior was observed for all peroxide modified test specimen. An example of the typical shape of the curves is represented in **Figure 28**, curves for different peroxide concentrations and temperatures are reported in **Appendix C**. The generation of a network causes finite extensibility of the chains, leading to an increased resistance against deformation at large strains. This presents itself as deviation from the linear viscoelastic regime, which is here defined as $3\eta_S^*$ (represented by the red line in **Figure 28**). At short timescales, there is an additionally observed deviation from the Trouton ratio. Although the origin of this effect is not studied here, it is likely an effect of the presence of crosslinks in the sample. Uniaxial extensional studies on polymer melts typically do not exhibit such behavior.

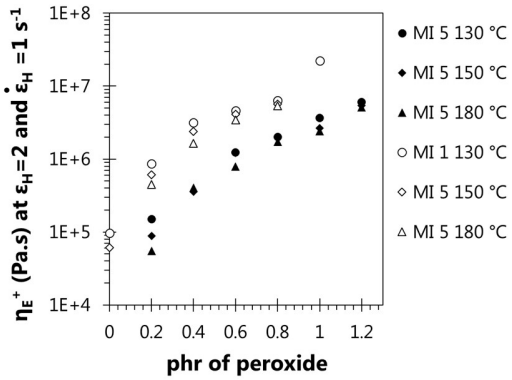

Figure 29: Extensional viscosity at ε_H=2 and $\dot{\varepsilon}_H$ =1 s^{-1} for INFUSE 9500 and 9100 as a function of the peroxide content.

The acting strain rate in a typical foaming experiment is approximately 1 s^{-1} and the Hencky strains are between 3 and 4 [36]. The extensional rheology is here summarized in **Figure 29** for each temperature at a strain rate of 1 s^{-1} and a Hencky strain of 2, since our samples often broke before a Hencky strain of 3 was reached. The maximum extensibility of the samples is represented in **Appendix C** Noteworthy is the apparent optimum in the maximum extensibility as a function of the peroxide content. This might be a result of increased brittleness as a result of crosslinking. The extensional viscosity of samples that could not reach ε_H=2 could not be represented in **Figure 29**. Similar to the observed trends of the shear rheology, the extensional viscosity of INFUSE™ OBC with a MI of 1 is generally higher than the extensional viscosity of the polymer with a MI of 5. It is also observed that the temperature dependence of the extensional properties is very moderate.

The strain hardening index was calculated according to the method as described in **Equation 29**, also at ε_H=2 and $\dot{\varepsilon}_H$ =1 s^{-1}. A general increase of SHI with peroxide content was observed, results at 150 °C are shown in **Figure 30**. Although it was not possible to measure the extensional behavior of the pure INFUSE™ 9500 due to its low viscosity, the pure resin of INFUSE™ 9100 was shown to lack strain hardening behavior. This is represented by a strain hardening index around 1. Within the statistical significance, the difference between the SHIs with respect to the MI is likely very moderate. For this reason, the magnitude of the extensional viscosity at relevant strain and strain rate as shown in **Figure 29** are thus concluded to be more illustrative, as a clear distinction can be made between different resin grades.

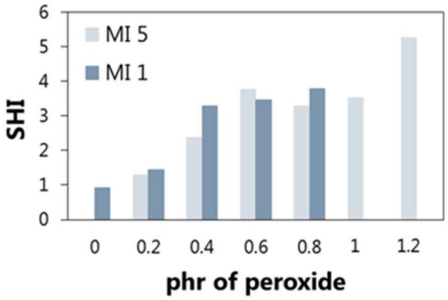

Figure 30: The strain hardening index (SHI) for INFUSE™ 9500 and 9100 as a function of the peroxide level at 150 °C, determined at ε_H=2 and $\dot{\varepsilon}_H$ = 1 s^{-1}

5.3 Representative rheological behavior

Due to the limited availability of uniaxial extensional characterization methods in generally well-equipped laboratory facilities, and the broader application of shear rheometer equipment, we were interested to find an evident relation between the shear complex viscosity of peroxide modified OBC at a particular frequency, and the representative uniaxial extensional viscosity. As shown in **Figure 31**, the representative extensional viscosity as defined in **paragraph 5.2.4** is plotted as a function of the shear viscosity at 0.1 rad/s at the corresponding temperature. The relation between this shear viscosity and extensional viscosity follows a power-law relation. This indicates that the shear viscosity can effectively be used as a prediction tool for the extensional viscosity, at least within this material family.

Similarly, the strain hardening index could be related with a power law relation to the tanδ at ω=0.1 rad/s. This confirms the equivalent scaling of the shear rheology at 0.1 rad/s and the representative extensional rheology for a foaming experiment. Although rheological properties in foaming are mostly dominated by extensional behavior, characterization of the shear rheology has thus been shown to suffice for analysis of foamability, foam structure and foam performance. In combination with the development of a tool to predict the viscosity of INFUSE™ 9500 in the thermoplastic regime based on the time temperature superposition principle as presented in **paragraph 5.1.1.1**, this indicates that once a foaming window has been defined, the foamability of a thermoplastic formulation of INFUSE™ OBC could be predicted by determining the viscoelastic behavior of the resin, rather than performing a foaming experiment.

Although the correlation of the extensional rheology to the shear rheology has been shown to exist for INFUSE™ OBC, it is unknown if other resin families behave with the same correlation. If in the future other resin families will be related to the foaming window as will be presented **Chapter 10**, it might be required to verify the identical scaling behavior, or to define the foaming window in terms of the extensional properties of the material.

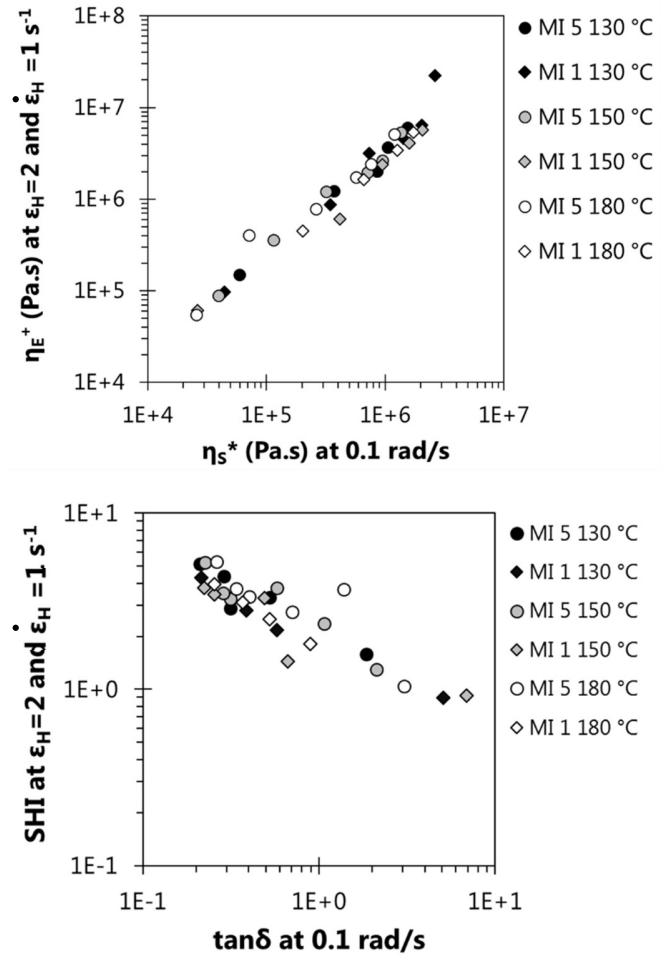

Figure 31: Top: representative extensional viscosity as a function of the shear complex viscosity at ω=0.1 rad/s. Bottom: strain hardening coefficient as a function of the tan at ω=0.1 rad/s.

6 Foaming

In this chapter, the methods that are employed in this work for production of foams by Crosslinked Injection Molding and One to One foaming are reported. The development pathway of the One to One Foaming is described in more detail in **Chapter 7.** Properties and morphology of the created foams will be discussed in **Chapter 8** and **9**. The formulations are described first as they are used in both methods, and accurately portray conventional formulations in terms of components.

6.1 Materials

Formulations for Crosslinked Injection Molding often consist of a standard set of components, which can be added in different amounts depending on the desired properties of the foam. The specific resin grades, peroxide masterbatch and blowing agent type can be varied, as well as the type and concentration of activator and filler. Based on the knowledge of foaming behavior in Crosslinked Injection Molding and the typical ratios employed in this method [39], a set of formulations has been designed for this project. For each formulation, here an equal filler and activator package and blowing agent concentration was added as described in **Table 4**. Similar to the peroxide Masterbatch, the used blowing agent Masterbatch Luvobatch BA 5332 consisted of 40% active Azodicarbonamide in granule form, it was provided by Arkema. As introduced in **Chapter 2.1.2**, ZnO and ZnSt act as the activators that drive the decomposition temperature of the azodicarbonamide down to match the foaming temperature of INFUSE™ OBC. For more information about the employed peroxide Masterbatch and the Roll Mill settings we refer to the method as described in **Chapter 4.2.1**. Compounding consisted of first completely melting the pure OBC resin on the roll mill and consequently adding ZnO and ZnSt. This also helped to minimize sticking of the resin to the rolls. After complete homogenization, the $CaCO_3$ was slowly incorporated and thoroughly mixed in the resin, after which the peroxide and blowing agent were added at the same time to minimize premature action at the compounding temperature.

Table 4: Formulations for Crosslinked Injection Molding.

Component	Parts/wt	Parts/wt	Parts/wt	Parts/wt	Parts/wt	Parts/wt
INFUSE™ 9100/9500	100	100	100	100	100	100
Luperox DC40P-SP2*	0.5	1	1.5	2	2.5	3
Luvobatch BA 5332**	5	5	5	5	5	5
ZnO	0.3	0.3	0.3	0.3	0.3	0.3
ZnSt	0.3	0.3	0.3	0.3	0.3	0.3
Omyalite 95T***	5	5	5	5	5	5

*Dicumyl peroxide masterbatch (40% active component)
**Azodicarbonamide masterbatch (40% active component)
***$CaCO_3$ powder

6.2 Crosslinked Injection Molding

As discussed in **Chapter** Fout! Verwijzingsbron niet gevonden.**,** Crosslinked Injection Molding is a method that is currently employed for foaming of OBCs, POEs, and EVA. Although the method is currently applied relatively often, the use of chemical blowing agents is no longer desirable in footwear applications and the lack of automation perspectives drives the industry to explore alternative fabrication methods.

6.2.1 **Method**

In Crosslinked Injection Molding, pelletized compounds are usually fed in the single screw injection unit and consequently injected in a heated mold. As in this project relatively small batches of compound are mixed, the pelletization and injection steps were evaded by using the Maingroup Injectionmolder Model E166S as compression molding machine. A mass of compound was first weighed to completely fill the mold volume. This compound was consequently heated for 10 minutes at 110 °C in an oven to soften. The hot mold (180 °C) was treated with silicone release agent, which was sprayed on the hot mold and consequently cured for 20 minutes to prevent sticking of the foam upon opening of the mold. The softened compound was then placed in the open mold, making sure that the mold surface was covered as well as possible. The mold was closed for 10 minutes to allow for curing and decomposition of the blowing agent under pressurized conditions. A vacuum was applied to ensure proper filling of the mold cavities. After 10 minutes, the mold was opened upon which the foam jumped from the mold. The foams expanded uniformly in all directions to dimensions much larger than the mold cavity. The foamed material was recovered and cooled in a fume hood.

6.2.2 **Discussion**

Standard formulations for this type of equipment typically have at least 2.5 phr of peroxide masterbatch (1 phr active peroxide) compounded into the resin. Here, compounds were thus foamed from high to low peroxide loading, since compounds with very low levels of peroxide were expected to remain unstable upon foaming. This hypothesis was confirmed, as samples with 0.6 phr active peroxide could not yield stable foams, both for INFUSE™ OBC 9100 and 9500. This instability is likely the result of poor extensional properties, in combination with very rapid expansion of the foam due to the high opening speed of the equipment. At these high rates, the nucleation density is very high and thin walls are stretched. When the extensional properties are insufficient, the walls cannot resist the stretch, and thus break, leading to deflation. It is expected that compounds with levels below 0.8 phr of peroxide could be foamed if the mold could be opened at lower velocities. The opening speed of the available machinery for CIM could here not be changed so the effect of the opening speed on the ultimate foam morphology and properties remains for future research. It is expected that by reducing the opening velocity of the mold, the nucleation density is reduced. This should result in in increased cell size and cell wall thickness, as the same volume of gas is available for less nucleation sites. Another way to successfully foam samples with relatively low levels of peroxide in the conventional process could be by adjusting the BA concentration. Lower BA concentrations will result in lower internal pressure, and thus also a more moderate expansion.

The other formulations (≥0.8 phr active peroxide) were foamed successfully, and were observed to improve in aesthetics upon successive foaming of multiple samples of the same formulation. Expansion ratios, although not quantified directly, increased visually with decreasing peroxide content. Foams of compounds of 5 MI INFUSE™ OBC also expanded more than samples of 1 MI INFUSE™ OBC. This already gives a first indication that the expansion ratio is determined by the viscosity of the material. In order to draw conclusions from the effect of the formulation on the cell size and cell size distribution, samples should desirably have the same density. It is known that the density could be controlled by varying the blowing agent concentration depending on the peroxide loading. Studying this effect was not possible within the timeline of this work.

6.3 One to One foaming

Based on a series of optimization procedures that are reported in **Chapter 7**, a method to approach the envisioned One to One Foaming procedure is defined. This includes the design of the mold, which was specifically fabricated for the purpose of this project, as well as the processing conditions. This method goes beyond the applicability of chemical blowing agents, and could be used as a simulation for physical foaming.

6.3.1 **Mold design**

Since prior to this project, there was no equipment available specifically intended for One to One foaming development, a simple mold was designed in cooperation with the workshop at Dow Chemical in Horgen. The design of the mold was inspired by a mold employed for foaming of thermoplastic resins as described by Laguna-Gutierez et al. [58]. In their approach, which is called 'Improved Compression Molding', pellets compounded with a chemical blowing agent are placed in a mold which is compressed in a hot-plate press above the decomposition temperature of the CBA. The top part of the mold is can move upward upon pressure release as a result of the growing foam, but the expansion ratio of the foam is controlled by hooks that constrain the upper mold plate. After full expansion of the foam, the mold is removed from the press and put in cold water to rapidly stabilize the thermoplastic foam. While the application of the mold in this work is vastly different, the mold employed in this work has taken a similar shape.

The design of the mold is considered Dow Confidential Information

6.3.2 **Method**

The developed foaming method is considered Dow Confidential Information

6.3.3 **Discussion**

The method as described here contributes to the research and development of automatization processes for athletic midsole fabrication in several ways. On the one hand, the industry is driving away from the use of chemical blowing agents. Experimental equipment for gas injection that are required for physical foaming are generally expensive. The method as presented here allows us to use a chemical blowing agent in the context of physical foaming. Physical foaming generally occurs at relatively low temperatures, since the gas saturation procedure does not occur at a high decomposition temperature. Here, the temperature can be controlled prior to the foaming action by cooling down the mold down from the decomposition temperature of the CBA after saturation of the polymer, to the temperature at which the material is optimally foamed. Testing of such cooling procedures in the mold as described here was not possible within the timeline of this project.

This study presents the first 'constrained' foaming experiments of (crosslinked) OBC-based resins. The method here was shown to be successful in providing samples with acceptable mold replication and surface aesthetics for a range of samples. These constraints limited us here to analyzing samples made with INFUSE™ OBC 9500. The strength of this method is the control over the density of the foam, which is not straightforward in CIM methods without adjusting the formulation. The properties of the produced foams will be reported in Chapter **8** and **9**.

7 Optimization of the One to One foaming Method

The development of a method for One to One foaming is innovative as constrained foaming of crosslinked OBC materials has not been reported before. The optimization steps consisted of finding the proper equipment, and taking measures to improve the aesthetical qualities of the foam, which were for the first time here crosslinked and foamed to its final dimensions inside a mold cavity.

Several types of equipment were used to test the mold and to determine the processing conditions to produce foams as envisioned. Optimization steps included improvement of the mold replication quality, and improvement of the aesthetical qualities of the foams.

The optimization steps of the foaming method are considered Dow Confidential Information

We were here unable to produce the entire range of samples as shown in **Table 4** for INFUSE™ 9100. The expansion ratio of the foam could be enhanced by increasing the loading of blowing agent, thus increasing the gas pressure to provide for bigger expansion of the cells. Although an extensive study was not within the scope of this work, we experimented here with doubling the blowing agent concentration to achieve a higher expansion ratio for the material with MI=1. In this case we could succeed in filling the mold successfully for a selection of samples. The performance of these foams was here not reported. This observation of significantly reduced expansion for lower MI samples raises questions for further experimentation with potentially even lower MI materials.

For INFUSE™ 9500 on the other hand, the whole range of samples was produced successfully. When the natural expansion ratio and mold volume were sufficiently in agreement, samples with smooth surfaces were obtained (**Figure 32**). The controllability of the expansion ratio of differently modified samples can be of interest for process optimization in future work. Correspondence of the natural expansion ratio of the foam, and the defined volume of the mold could be achieved by modifying the blowing agent concentration for differently crosslinked formulations.

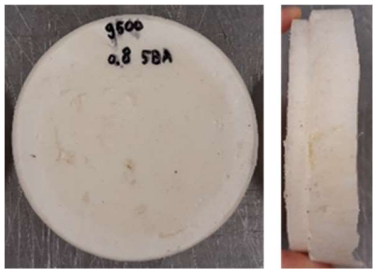

Figure 32: Example of One to One foamed sample after process optimization.

7.1 Nucleation improvement

As footwear foams have typically relatively small cell size (<250 µm), we experimented here with the addition of nucleating agents to the formulations of **Table 4**. The objective was to yield lower cell sizes for well nucleated samples, which has been related to performance improvement of the foam, especially in terms of compression set performance. Upon addition of nucleating agent, heterogeneous nucleation should theoretically be enhanced. Homogeneous nucleation could be enhanced by modifying the processing procedure.

Such control over the homogeneous nucleation would require optimization of specialized equipment which was in this work not available. Some experiments for heterogeneous nucleation improvement were performed by adding nucleating agents to the formulations of **Table 4** for application in One to One foaming. Nucleating agents NX-8000 and HPN-20E from Milliken® were added to the formulations at 0.2 and 0.1 wt% respectively. These amounts were chosen on advice of Milliken®.

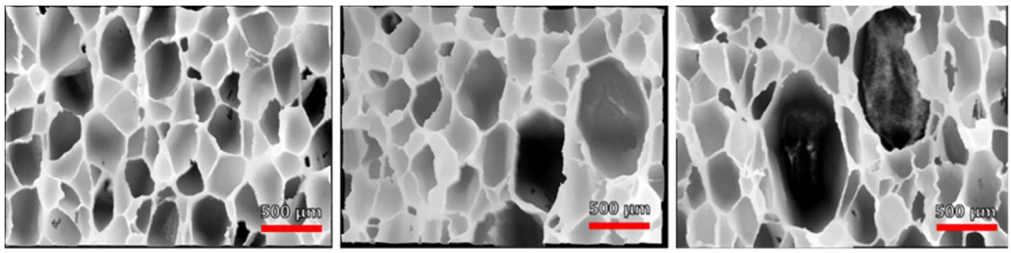

Figure 33: Comparison of cell structure of INFUSE™ 9500, compounded according to **Table 3** with 0.8 phr of peroxide and two different nucleating agents. Foams with added nucleators contained significant amounts of large voids.

Large bubbles were observed in the middle of the foam in samples with added nucleating agent. Microscopy images of a comparative study between samples of INFUSE™ 9500 compounded according to **Table 4** with 0.8 phr peroxide and the described amounts of nucleator are represented in **Figure 33**. The method for acquiring such images is described in **paragraph 8.3**. The reason for the generation of large voids as a result of addition of nucleating agents is unknown. The microscopy images were analyzed as described in **Chapter 8** to get a description of the cell size and cell size distribution of the samples. The results of this study are reported in **Appendix D** and summarized in **Table 5**. Despite the generation of large voids, the average cell size reduced upon addition of HPN-20E to the formulation. In the cell size distribution, there is a spike for bubbles with a size between 150 and 200 µm. Addition of NX-8000 to the formulation did not improve the cell size or distribution, as a larger average cell size was measured. In future work, one could experiment with different types and concentrations of nucleator to study the effect on the cell size in more detail. All samples in later chapters were prepared without the addition of nucleating agents.

Table 5: Average cell size determined by image analysis for formulations of INFUSE™ OBC with MI=5 Samples were compounded according to **Table 4** with 0.8 phr of peroxide and two different nucleating agents.

Sample	Average cell size (µm)	Standard deviation (µm)
No added nucleator	249	122
HPN-20E	242	133
NX-8000	254	133

8 Foam morphology

An analysis of the foam morphology was performed on both crosslinked injection molded samples and One to One foamed samples. These properties include morphological characteristics such as: cell size, cell size distribution and aspect ratio of the bubbles, which were determined from image analysis of laser microscopy images. The analysis also included determination of the foam density with and without skin. This helps to understand to what extent the foam properties are affected by the processing method in terms of cell size and orientation. The aim is to understand these differences in performance and aesthetics, and to define a foaming window for the employed methods.

8.1 Sample preparation

Since the two foaming methods yielded foams of very different sizes and thicknesses, the sample preparation was not identical for the differently prepared samples. Samples were used first to perform microscopic imaging, as the cross-sections were of sufficient quality. After imaging, the samples were used to determine the foam density. Samples were always created 24 hours after foaming to ensure relaxation of the foam structure. Small foam blocks were punched from different locations across the samples (**Figure 34**) depending on the applied foaming method.

8.1.1 **Crosslinked Injection Molded samples**

For the foams created by CIM, which yielded large rectangular foams, a square cutting die with dimensions 21x23 mm was used to punch samples from the foam sheet. Three samples were taken both before and after skin removal with a FORTUNA sole slicer.

8.1.2 **One to One foamed samples**

As the One to One foamed samples were initially too thick to be placed under the cutting dye, rectangular test specimen were cut manually with the sharp blade of an IDEAL trimmer. A slice of approximately one centimeter in thickness was taken at least one centimeter from the foam border. The slice was taken in the plane of the thickness direction, and consequently divided in at least three similarly sized blocks. Samples were not taken from the center of the foam as the limited foam dimensions required the middle of the foam to be intact for other characterization methods. After skin removal and thickness reduction of the remaining foam sample, now the 21x23 mm cutting die was again used to prepare samples without skin.

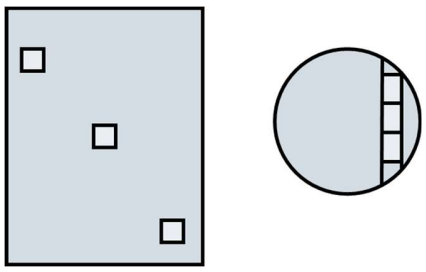

Figure 34: Schematic representation of sample distribution. Left: CIM samples, right: One to One foamed samples.

8.2 Density

8.2.1 **Immersion method**

The density of previously described samples was measured according to ASTM standard D-792 by water immersion of the foam samples. Dry samples were first weighed in air on electronic scales. Then in between each sample, a cup of de-ionized water was placed onto the scales and a needle was lowered into the water. The system is calibrated by tarring the scales. A foam sample was attached to the needle and immersed into the de-ionized water. The weight of the sample in the water was recorded, which is representative for the displaced volume of water by the foam sample. The average weights of three foam specimen from one complete foam yield the density via the following relation:

$$\rho = \frac{Average\ weight\ in\ air}{Average\ weight\ in\ deionized\ water} \tag{30}$$

8.2.2 **Results**

The recorded densities for successfully produced CIM samples were here reported as a function of the shear complex viscosity at 0.1 rad/s at the corresponding foaming temperature (180 °C). As shown in **Figure 35**, the density for samples without skin is somewhat smaller, but the observed trends are not different. It becomes immediately obvious that the density is largely determined by the viscosity of the (crosslinked) network. A linear increase in foam density is observed upon increasing the representative viscosity as a result of modification of the base resin with peroxide. This effect is also in accordance with the previously observed decrease in expansion with increasing peroxide content. Based on these results, the density of a foam produced by the traditional foaming method can be predicted by rheological characterization of the resin as reported in **Chapter 5**. Besides, this relationship also defines in part the foaming window in terms of extensional and rheological properties for foams created by the traditional method. It is now observed that in order to create a stable foam with this process, a minimal resin viscosity of approximately 6 x 10^5 Pa.s at 0.1 rad/s is required to create a stable foam, the upper side of the spectrum is then defined by the maximum tolerable density of the foam.

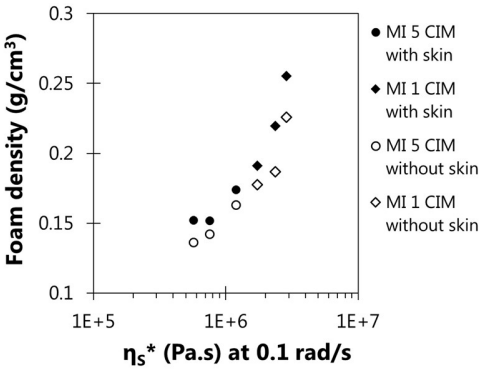

Figure 35: Foam density of CIM samples with and without skin.

Although the method employed in One to One Foaming should allow for control over the density, it becomes apparent from **Figure 36** that there is a slight variation in the density across the samples. The density was observed to decrease considerably upon skin removal. Nevertheless, the results are promising as they indicate that foams with relatively low levels of crosslinking can be produced that still have suitable densities for midsole applications if the material preservation inside the mold is optimized. It is expected that the skin thickness can be reduced by optimizing the expansion ratio of the formulation to the mold volume by adjusting the concentration of blowing agent and changing the opening speed of the mold.

The density as measured by the immersion method for the lowest modified (but not thermoplastic) sample, with 0.2 phr peroxide foamed at 180 °C, is unexpectedly high. Based on the previously reported limitations of achieving sufficiently high densities for lightly crosslinked samples, a lower density would have been in line with the effects observed. An incorrectly high density measured by the immersion method could result from a high open cell content in the foam. If a foam absorbs a lot of water, the volume of displaced water appears lower. At the same dry weight, this results in the observation of an apparent high density. This generation of open cells in a lightly crosslinked sample effectively confirms the necessity of sufficient extensional properties in order to provide the foam stability, but also to retain closed cells. The quantification of the open cell content remains as a recommendation for future work, as the presence of open cells is undesirable in midsole applications.

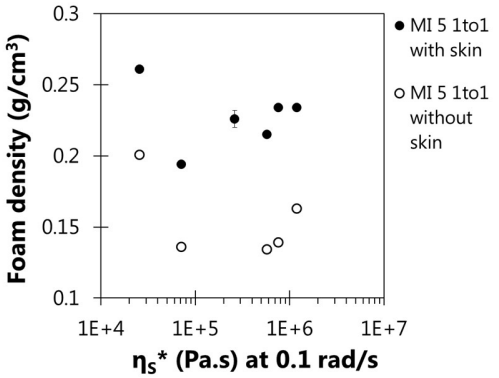

Figure 36: Foam density of One to One foamed samples with and without skin.

8.3 Cell analysis

8.3.1 **Image acquisition**

A confocal laser scanning microscope (Keyence VK-X260K) for 3D and profile measurements was equipped with a 10x/0.3 magnifying lens. All image acquisition was performed in Surface Profile mode with high accuracy quality and a standard resolution of 1024x768 pixels. As the cell sizes of the constrained foams were relatively large and there was no 5x magnification lens available, an automatic stitching procedure was performed to create a 2x2 stitched image of 1920x1441 pixels to provide a sufficient quantity of cells.

Prior to measuring the density of the foams, the density samples were used to create images for the cell size analysis as they had suitably smooth and well defined surfaces along the cutting surface. From each foam, three samples were imaged to obtain enough statistics. Images were taken in the plane parallel to the growth direction in the center of the foam slice. The samples were thus always placed in the same orientation, with the skin sides on the top and bottom of the picture.

After image acquisition, filtering steps in the Multi File Analyzer v.2.1.2.17 software (Keyence) were required to obtain images with sufficient contrast for analysis (**Figure 37**). Depending on sample cutting quality, a plane fit correction was usually sufficient to correct any incline. For more difficult surface profile adjustments, surface shape corrections were recommended. User defined profiles can be specified in the secant curved surface (Image processing tool in surface shape correction tab) to eliminate height curvature. Subsequently, the images were converted to gray scale pallet and exported as an image format.

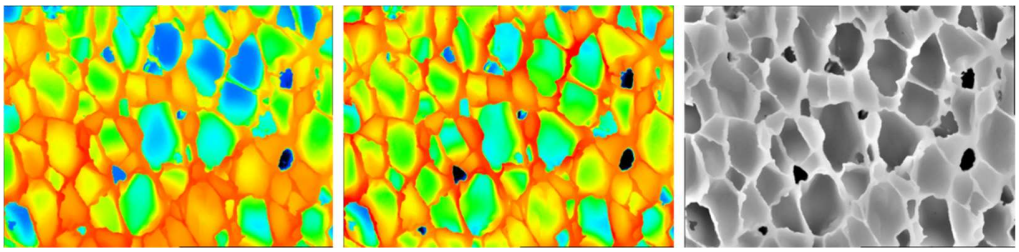

Figure 37: From left to right: image recorded directly with microscope, picture after surface shape correction, picture after setting height display to greyscale.

8.3.2 **Image analysis**

Two separate macros in FIJI software were developed and used to analyze the cell sizes, cell size distributions and aspect ratios. The foams that were created with the traditional Crosslinked Injection Molding method were analyzed with a macro that assumed thin cell walls and had a slightly lower cell size threshold. As One to One foamed samples have relatively large bubbles, a thicker cell wall was accounted for. Both macros follow several identical filtering and thresholding steps that were needed for bubble segmentation, the specific scaling and filtering procedure was described in a separate CRI report. These steps automatically lead to an interactive step where, if necessary, any missing cell walls could be manually drawn in (**Figure 38**). After verification

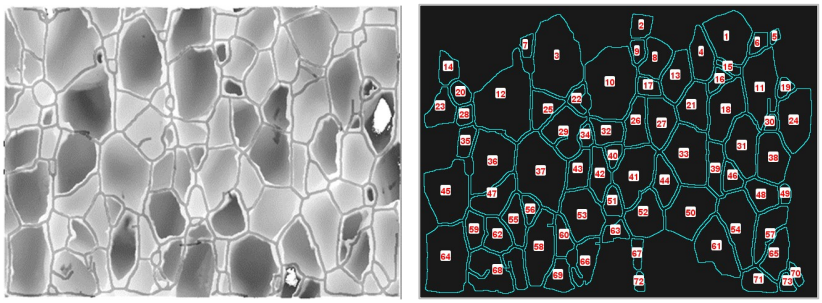

Figure 38: Left: manual step after filtering where in grey, any insufficiently segmented pore can be drawn in. Right: final segmentation and numbering of the pores.

whether all cells were correctly segmented, any unsatisfactory separated cells could be removed from the table.

Output of the macro includes a collection of parameters such as the area, various size descriptors and shape descriptors. The most representative descriptors were used here to define the cell size, cell size distribution and aspect ratio of the cells. Since the bubbles are generally not perfectly spherical, the aspect ratio represents well how much the bubbles are elongated. The aspect ratio of the bubbles is determined by the macro by fitting an ellipse to a segmented bubble, and defining the major and minor axis of the ellipse (**Figure 39**). The aspect ratio of the bubble follows from:

$$AR = \frac{[major\ axis]}{[minor\ axis]} \tag{31}$$

In order to describe the size of an anisotropic particle, here the distance between the two focus points, defined here as the 'cell size' was chosen. An ellipse has two focus points, which lie on the major axis with equal spacing from the ellipse center. For any point on the ellipse, the sum of the distances to the foci are always the same. An ellipse is partly defined by the location of the foci with respect to the ellipse center (the focal length), which can be calculated if the major and minor axis lengths are known. We define here the distance between the two foci as the cell size, which corresponds to twice the focal length.

$$Cell\ size = 2\sqrt{\left(\frac{1}{2}[major\ axis]\right)^2 - \left(\frac{1}{2}[minor\ axis]\right)^2} \tag{32}$$

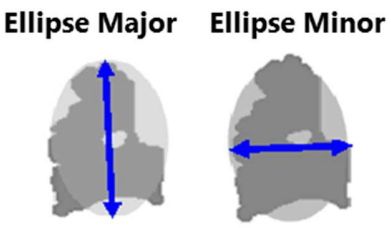

Figure 39: representation of the major and minor axis of an ellipse fitted to a segmented bubble.

8.3.3 **Results**

Based on the previously described procedures, the cell size and aspect ratio distributions for the foams were determined. From these distributions, also the average cell sizes and average aspect ratio were calculated to study the foam structure.

8.3.3.1 Cell size

The histograms that represent the cell sizes that were found in samples that were produced with the traditional Crosslinked Injection Molding method are represented in **Appendix D**. The corresponding average cell size and standard deviations are shown in **Table 6**. It becomes immediately apparent that all foamed samples have a relatively narrow cell size distribution with a peak around 110 micron. Upon analysis of the average cell size and standard deviation, it is shown that modification with increasing amounts of peroxide leads to a decreasing cell size. This effect corresponds to the observed trends in the density. Samples with more densely crosslinked structures appear to resist more against the expansion, leading to higher densities and lower cell sizes. There are suggestions that increased homogenization represented by the moderate decrease of the standard deviation could be a function of the extensional behavior, since the events that lead to the formation of large cells are then evaded [58].

Table 6: Average cell size and standard deviations of CIM foams.

Sample	Average cell size	Standard deviation
MI 1		
0.8 phr peroxide	124.3	70.9
1 phr peroxide	115.8	60.3
1.2 phr peroxide	103.5	64.2
MI 5		
0.8 phr peroxide	120.3	68.5
1 phr peroxide	106.9	59.9
1.2 phr peroxide	94.5	58.1

Although the cell size of One to One foamed samples is generally larger, similar trends were observed in One to One foamed samples of which the histograms are shown in **Appendix D** and the average cell sizes and standard deviations are reported in **Table 7**. Here, cell sizes also decrease considerably with peroxide concentration, and distributions become more narrow with increasing peroxide concentration.

The distributions for One to One foamed samples are relatively large with respect to the CIM foams. Since the employed formulations are identical, and the extensional properties correspond, this effect is likely an effect of the processing conditions. With only few nucleation sites but the same gas pressure, cells will grow to larger volumes and apparently also with a broader variety.

Table 7: Average cell size distance and standard deviations of One to One foamed samples.

Sample	Average cell size	Standard deviation
MI 5		
0.2 phr peroxide	277.2	153.8
0.4 phr peroxide	256.9	145.2
0.6 phr peroxide	229.1	117.5
0.8 phr peroxide	248.6	121.8
1 phr peroxide	206.4	98.3
1.2 phr peroxide	178.4	89.5

The general effect of the extensional properties on the bubble size is inspected by plotting the average cell size as a function of the representative shear complex viscosity as determined in **paragraph 5.3** for the corresponding samples (**Figure 40**). Although very different cell sizes are found for the respective foaming methods, the effect of extensional properties is clear; an increase in extensional viscosity as a result of peroxide modification results in a decrease in cell size. If the samples would have been produced with the same density and amount of homogeneous nucleation, irrespective of the foaming method, a more illustrative comparison between the cell sizes could be made. Nevertheless, it has been shown that even samples with relatively small amounts of crosslinking, and correspondingly low viscosities can succesfully be foamed to cell sizes around 250 µm, which are in a suitable range for midsole applications. Foams in the thermoplastic regime were here lacking.

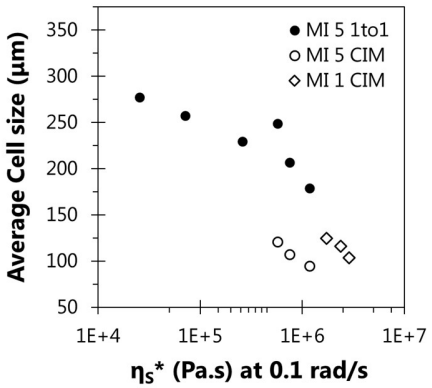

Figure 40: Average cell size of One to One foamed samples and Crosslinked injection molded samples.

8.3.3.2 Aspect ratio

By inspecting the average values of the major and minor axis of the bubbles for the respective samples, it is found that the bubbles are generally not circular. Although there appears to be a linear relation between the major and minor axis of the observed cells (**Figure 41**), the axes are not of equal length. The histograms related to the aspect ratio of the produced foams, as well as

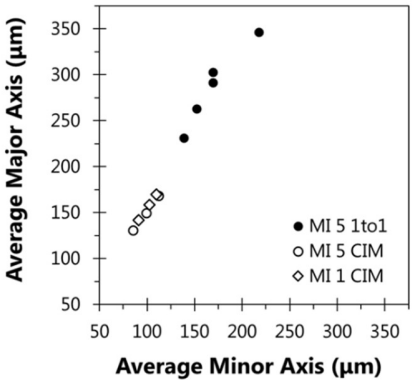

Figure 41: Average Major axis as a function of the average minor axis. This illustrates the anisotropic nature of the bubbles.

the tables describing the average AR and standard deviation can be found in **Appendix D.** Similar to the trends observed for the cell size and cell size distribution, the aspect ratios of One to One foamed samples are larger than that of CIM samples.

The width of the distribution is also larger. The trend in the average aspect ratio as a function of the representative viscosity is here represented in **Figure 42**. Among the CIM samples, there appears to be an increase in the aspect ratio relative to the representative peroxide concentration. The origin of this effect in not easy to pinpoint and comparison with One to One foamed samples is difficult since the expansion ratio and expansion directions are vastly different. Since in CIM samples with relatively high viscosity also yield lower densities, the aspect ratio might be affected by the expansion direction. The observed cell sizes and aspect ratios will be used in **Chapter 9** in relation to the mechanical properties of the foams.

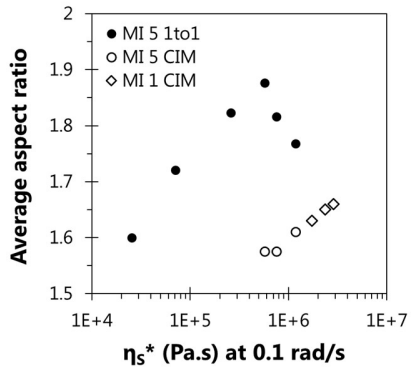

Figure 42: relation of the average aspect ratio of CIM samples with respect to the representative viscosity.

9 Mechanical analysis

Based on the rheological and morphological characterizations of the produced foams, the effect on the performance was analyzed to eventually evaluate the necessity of a post crosslinking step. The benchmark for foam performance was described in **paragraph 2.4** and typical performance requirements are here used as a reference for the observed foam properties.

9.1 Rebound resilience

9.1.1 **Methods**

The rebound resilience was measured according to ASTM D-3574. A foam sample was placed underneath a tube with inner diameter 42 mm with indicated scale. A metal ball of 16 mm in diameter was dropped onto the sample. If the ball bounced back without touching the side of the cylinder, the height of the bounce was recorded. An average of five successful bounces was recorded for each sample.

9.1.2 **Results**

The most noteworthy effect of the foam morphology in relation to the footwear performance was observed in the rebound resilience (**Figure 43**). While the rebound has often been related to foam softness, it was here shown to be linearly dependent on the average aspect ratio of the bubbles. The rebound resilience is in footwear an important measure for the energy return, and a significant decrease in rebound as a result of the increased elongation of the cells as a result of confined foaming is unfavorable. In general, the direction of elongation was in the direction of the foam growth. It is currently unknown how the bubble orientation affects the rebound properties.

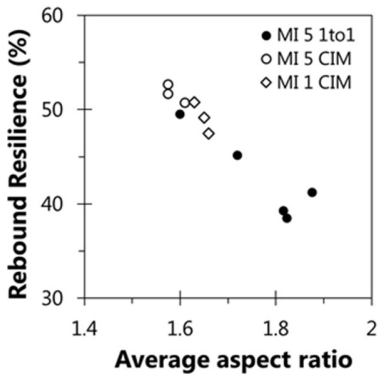

Figure 43: Rebound resilience as a function of the average aspect ratio.

9.2 Compression set

9.2.1 **Methods**

Compression set is usually measured on foams without skin, the skin of a foam can be removed with a FORTUNA sole slicer. As the initial thickness of the One to One foamed samples was too large to be cut with the sole slicer immediately, the sample was first cut in half with a band saw in

the direction perpendicular to the growth direction. Consequently, the skin was removed from the outer sides with the sole slicer. From CIM samples the skin was removed from the complete foam sheet. In agreement with the compression set measurement standard ASTM D-3574, the samples were reduced to a thickness of 9.4 mm and consequently cut into disks with a 28 mm diameter cutting die. The thickness of the samples was measured with a broad footed tabletop caliper tool. As the soft foams sometimes showed a slight deviation in thicknesses across the sample, the thickness was always determined in the middle of the sample disk.

The samples were then compressed 25% with respect to the initial sample thickness for a duration of 24 hours at room temperature. 30 minutes and 24 hours after decompression of the foam specimen, the thickness was again measured. Compression set was determined for 3 test specimen per foam and averaged.

9.2.2 **Results**

The measured compression set 30 minutes and 24 hours after decompression are represented as a function of the cell size in **Figure 44**. Although the compression set of a material is often related to the cell size or cell wall thickness of a foam, the compression sets, especially 24 hours after decompression, were observed to be very low. The compression set 30 minutes after decompression seems to vary somewhat with cell size, though the One to One foamed samples show a relatively low compression set. Performing these experiments at elevated temperature should help in formulating definitive conclusions. It could be useful to also quantify the open cell content of all foams, since a low compression set can sometimes be a result of a high open cell content.

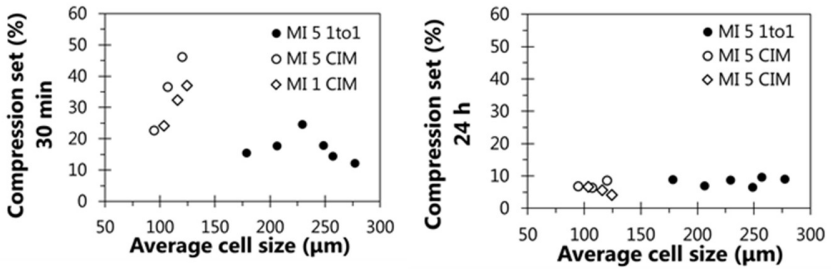

Figure 44: Compression set measured at room temperature, 30 min and 24 h after decompression.

9.3 Hardness

9.3.1 **Methods**

Measuring the hardness of a foam is a straightforward procedure that can be done on any foam sample or scrap piece of at least 6 mm in thickness at least 12 mm from the edge of the foam sample. The hardness was measured with two methods that are generally good at quantifying the hardness of soft rubbers and foams. The hardness of the materials was determined according to standard ASTM D2240. An average of five readings was used.

9.3.2 **Results**

The results of the Shore A hardness are represented in **Figure 45** as a function of the foam density, Asker C hardness is shown in **Appendix E**. In line with the commonly observed trend, hardness increases linearly with increasing foam density. With respect to the typical hardness as required for optimal midsole performance and comfort (Asker C 45-60, Shore A 22-34), the observed hardness here is relatively low for most of the crosslinked injection molded samples. In an optimized One to One foaming method the density is controlled, which means that foams with desirable hardness could be made readily once the polymer has been selected.

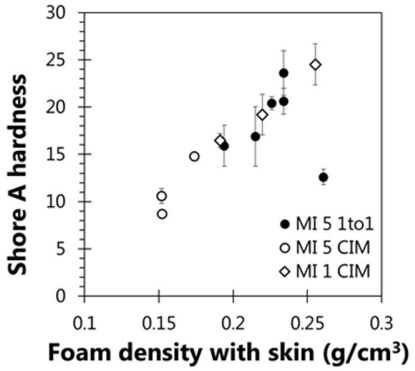

Figure 45: Shore A hardness of foams with skin as a function of the foam density.

9.4 Split tear

9.4.1 **Methods**

Slit tear was performed according to the SATRA TM 65 Standard. Split tear samples were prepared by cutting samples of 25x75x5 mm without skin. A slit of 16 mm was cut in the center of the sample. For each sample a pre-load of 0.5 N was used and the split speed of the measurement was set to 100 mm/min.

9.4.2 **Results**

The results for split tear are shown in **Figure 46**. It was observed that the split tear increases with increasing formulation viscosity. This would suggest that a post-crosslinking step with silane chemistry could further improve the split tear behavior of the samples, especially for samples which are modified with very low levels of peroxide. The split tear of the One to One foamed samples was observed to be slightly higher than that of crosslinked injection molded samples at the same modification and Melt Index. The foaming methodology has thus not negatively affected this property.

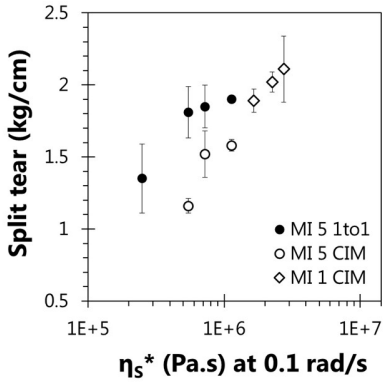

Figure 46: Split tear as a function of the representative viscosity

10 Foaming window

Based on the rheological characterization of the footwear formulations, and the correlation between the representative extensional properties and the shear viscoelastic behavior at 0.1 rad/s, a foaming window for INFUSE™ OBC was constructed for the developed One to One foaming process (**Figure 47**). In this representation the extensional properties of the material improve in the bottom-right direction. The foaming window has been defined based on the successfully foamed samples of INFUSE™ OBC with MI=5 with formulations as shown in **Table 4**. Successful foaming was here defined as the generation of a foam with suitable density, cell size and no clear indication of high open cell content. Further experimentation can lead to the optimization of the exact boundaries of the window, the window is left out in **Figure 47** because it is considered Dow confidential Information.

The experimentally observed thermoplastic samples, which were here defined as the samples that could be fitted by the time temperature superposition principle, are represented in red. In this work, the possibility of foaming in the thermoplastic regime has not been validated.

Interpretations of the foaming window are considered Dow Confidential Information

For uncrosslinked polymers, it is expected to be challenging to arrive without modification at a low tanδ, this would relate to the absence of strain hardening behavior for such pure melts. In future research, other polymer families or intrinsically strain hardening thermoplastic materials might be related to this foaming window. It is however currently unclear if the correlation between the representative extensional viscosity and the shear complex viscosity at 0.1 rad/s at corresponding temperature exists for all polymer families. It is recommended to study the existence of this correlation for other resin families. While the use of the shear rheology in relation to the foaming window is preferred due to the experimental simplicity of the test, the foaming window in terms of extensional properties can also be used if the correlation is absent for other polymer families (**Figure 48**).

The location of the foaming window is expected to shift as a result of modifications to the process (set expansion ratio, degree of nucleation) or the formulation (amount of blowing agent). This is supported by the observations during experimentation in Crosslinked Injection Molding, of which the window was observed to have a different location. Once a process has been defined, and an expansion ratio has been chosen, the location of the foaming window can be again tailored to the processing conditions.

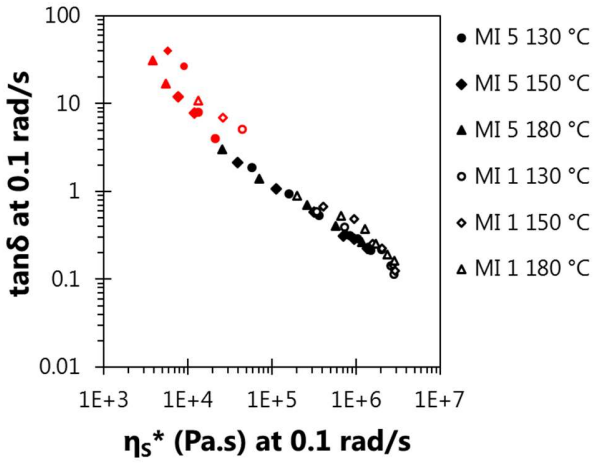

Figure 47: The foaming window for One to One Foaming, constructed for INFUSE™ OBC based on the correlation between shear and extensional behavior. *The boundaries of the foaming window have been removed here due to confidentiality.*

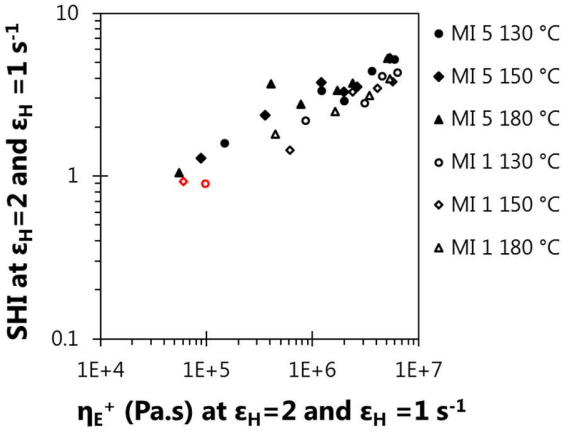

Figure 48: the foaming window for One to One constructed for INFUSE™ OBC based on the extensional behavior. *The boundaries of the foaming window have been removed here due to confidentiality.*

11 Conclusions and outlook

11.1 Conclusion

The curing kinetics of OBC were shown to be unaffected by the peroxide concentration and MI in the studied regime. The observed activation energy was approximately 160 kJ mol^{-1} and the rate constant and curing times were modeled as a function of temperature. This analysis has enabled us to produce compounds with different levels of peroxide in a reproducible way. Based on shear rheology, two regimes were observed, a thermoplastic regime at low crosslink-density and a rubbery regime with corresponding temperature independence at high peroxide modification. Thermoplastic (lightly peroxide modified) samples were shown to follow the time temperature superposition principle which led to the design of a model that allows the viscosity at any temperature, frequency and peroxide concentration below 0.1 phr to be extracted for OBC (MI=5) in the thermoplastic regime. By uniaxial extensional rheology, the strain hardening (SH) nature of all peroxide modified samples was confirmed. An increase in SH behavior was a result of higher peroxide concentration. For INFUSE™ OBC, a correlation was found between the uniaxial extensional viscosity that is representative for foaming conditions (ε_H=2 and $\dot{\varepsilon}_H$ =1 s^{-1}) and the shear complex viscosity at 0.1 rad/s at corresponding temperature.

The development of a 'One to One' foaming technique in which a polyolefin elastomer (POE)-based midsole foam is formed inside a mold cavity is crucial for the automation perspective of athletic footwear since it allows several footwear components to be attached in a single step. Such a method could effectively replace the traditional Crosslinked Injection Molding method, in which a foam expands outside of a mold cavity, which then requires manual adhesion to the remaining shoe components. Based on several optimization procedures, OBC was here foamed to suitable density and cell size inside a mold cavity providing suitable surface aesthetics.

The density of the foams was effectively controlled. The development of an automated image analysis tool for confocal laser microscopy images resulted in the characterization of the cell size, cell size distribution and aspect ratio of the foams. In terms of mechanical properties, the compression set was observed to be generally low and the density controlled the hardness of the foams. Since the mechanical properties of One to One foamed samples created with lower levels of peroxide were largely determined by the foam density and cell morphology, a post-crosslinking step with silane might not be required to arrive at optimal midsole performance. The property that can possibly improve by a silane post-cure is split tear, which was observed to improve with resin viscosity, or therefore with crosslink density.

11.2 Outlook

When other polymer families, possibly with intrinsic strain hardening properties in the thermoplastic regime, are in the future tested for applications in One to One foaming, the correlation between the shear and extensional rheology should be confirmed. When the foamability of thermoplastic resins within the optimized foaming window is confirmed, and the absence of open cells is tested, experimentation with peroxides with lower decomposition temperatures will be valuable, especially in combination with physical blowing agents.

The effect of the plastization effect of supersaturated melts as a result of blowing agent decomposition can be quantified with an RPA with a closed chamber. This can potentially lead to the clarification of the effect of the resin viscosity and gas pressure for different formulations on the natural expansion ratio of the foam. This should also aid in the understanding whether foams of lower MI could ever reach the desired density for midsole foams. The effect of the pressure drop rate on the nucleation density should then also be quantified and optimized for desired foam properties. The rate of the pressure drop will also affect the cell size, and likely also the foaming window in terms of foam stability. Since in this work the amount of homogeneous nucleation in One to One foaming experiments and Crosslinked Injection Molding methods are vastly different, it is difficult to make a representative comparison between the observed cell sizes. By varying the blowing agent concentrations or pressure drop rates, One to One foamed samples can potentially be made with corresponding (nucleation) density to Crosslinked injection molded foams. This might allow for more representative morphology changes as a result of the employed methods. The nucleation density can potentially be increased similarly with nucleating agents.

Based on the observations of the effect of foaming method on foam morphology, there are several details that require further research. The elongation of the cells was shown to affect the mechanical behavior of the foam. The effect of the orientation of these elongated cells might allow the utilization of controlled cell orientation for increased performance. Although the mold replication was observed to be good for the created foams, midsole foams generally have some surface definition and patterning for aesthetical qualities. Incorporation of surface definition that is representative for midsole foams might help in quantifying the mold replication quality of the foams.

Exploration of the automation perspectives as a result of the conclusions of this work, and the future verification of the foamability of thermoplastic resins might lead to different automation scenarios. There are several hypothesized methods for automation:

The automation perspectives are considered Dow Confidential Information

12 Acknowledgments

This work has benefitted greatly from the many collaborations that were possible within Dow. Gratitude goes out to Miguel Prieto, who has been an inspiration throughout the project and has contributed many of the ideas as presented in this work. Under the technical coaching of Jef van Dun, collaboration with international experts was supported and the work was elevated towards a cohesive and globally oriented result. Thanks to the industrial and academic experience of Jaap den Doelder and our enjoyable discussions, the work was placed in a context that is of both academic and industrial value.

The shared interest and enthusiasm for rheology with Sylvie Vervoort encouraged me to explore the versatile nature of these methods. Our discussions were as educational as they were motivating. Ewa Tocha contributed much to this work by employing her expertise to ultimately develop an image analysis tool in a short timeframe. The interactive and creative nature of our collaboration was always very pleasant.

The technical support has benefitted this work tremendously. The trainings for the range of used equipment increased the multidisciplinary nature of this work. Elias Manetsberger is thanked for his assistance throughout the project. Thomas de Wilde is thanked for his experimental contributions to the extensional rheology chapter. Monika Plass, Ramona Bernet and Moni Enzenberger are thanked for their assistance in the analytical lab.

The general interest of the international colleagues are greatly appreciated. Especially Lv Bo is thanked for his help to place the proceedings of the work in perspective of current footwear innovations.

I would like to thank Michael Chen, Enrique Torres, Barbara Bonavoglia and Patrizia Napoli for their personal support. Though many more people contributed to the welcoming feeling I experienced in the team. The close interaction with the lab staff, TS&Ds and students made this an unforgettable experience.

13 References

1. Drenckhan, W. and A. Saint-Jalmes, *The science of foaming*. Advances in Colloid and Interface Science, 2015. **222**: p. 228-259.
2. Zhang, Y., *Polyolefin formulations for improved foaming: effects of molecular structure and material properties*. 2013, Queen's University: Kingston, Ontario, Canada.
3. Kong, H.J., et al., *Investigation of thermoplastic elastomer (TPE) foaming process using blowing agent by rheological and morphological methods*. Journal of Applied Polymer Science, 2019. **136**(8): p. 47358.
4. Gama, N.V., A. Ferreira, and A. Barros-Timmons, *Polyurethane Foams: Past, Present, and Future*. Materials (Basel, Switzerland), 2018. **11**(10): p. 1841.
5. Bhuvaneswari. G, H., *3 - Degradability of Polymers*, in *Recycling of Polyurethane Foams*, S. Thomas, et al., Editors. 2018, William Andrew Publishing. p. 29-44.
6. McCormick, J.A., et al., *Tailored rheology of a metallocene polyolefin through silane grafting and subsequent silane crosslinking*. Journal of Polymer Science Part B: Polymer Physics, 2000. **38**(18): p. 2468-2479.
7. Low, B.T., *Development of Polyolefin based foamed midsole for footwear applications*. 2009, Dow CRI Report - 2009004999
8. Kummer, K., G., et al., *Processing and Performance Attributes of Olefin Block Copolymers in Crosslinked Foams*. 2014, The Dow Chemical Company.
9. Van Dun, J., et al., *Advanced Manufacturing in Footwear: The Need for One-to-One Foaming*. 2017, Dow CRI Report - 2017002252
10. Brückner, K., et al., *Polyurethane-foam midsoles in running shoes - impact energy and damping*. Procedia Engineering, 2010. **2**(2): p. 2789-2793.
11. Burley, A.C., *Toward a Fundamental Understanding of Bubble Nucleation in Polymer Foaming*. 2012, PhD Thesis, The Ohio State University.
12. Gendron, R. and M. Champagne, *Effect of Physical Foaming Agents on the Viscosity of Various Polyolefin Resins*. Journal of Cellular Plastics, 2004. **40**: p. 131-143.
13. Reyes-Labarta, J.A. and A. Marcilla, *Kinetic study of the decompositions involved in the thermal degradation of commercial azodicarbonamide*. Journal of Applied Polymer Science, 2008. **107**(1): p. 339-346.
14. Stehr, J., *Chemical Blowing Agents in the Rubber Industry. Past – Present – and Future?* International Polymer Science and Technology, 2016. **43**(5): p. 1-10.
15. Krutko, I., I. Danylo, and V. Kaulin, *Kinetics of azodicarbonamide decomposition in the presence of an initiator for obtaining solid foams*. Voprosy Khimii i Khimicheskoi Tekhnologii, 2019: p. 26-34.
16. Exelby, J.H., et al., *Formulating Expanded Products*, in *Handbook of Vinyl Formulating*. p. 379-391.
17. Throne, J.L., *Thermoplastic Foam Extrusion: An Introduction*. 2004
18. Lee, Y.-D. and L.-F. Wang, *Properties of polypropylene structural foam crosslinked by vinyltrimethoxy silane*. Journal of Applied Polymer Science, 1986. **32**(4): p. 4639-4647.
19. Bhatti, A.S., et al., *The thermal decomposition of azodicarbonamide*. Thermochimica Acta, 1984. **76**(1): p. 63-77.
20. Kummer, K., et al., *2015 Footwear Foam Training in Shanghai Dow Center*. 2015, Dow CRI Report - 2015006686

21. Okolieocha, C., et al., *Microcellular to nanocellular polymer foams: Progress (2004–2015) and future directions – A review*. European Polymer Journal, 2015. **73**: p. 500-519.
22. Mokhtarimotamenishirvan, M., N. Famili, and A. Golbang, *A Review on the Application of Nucleation Theories in Thermoplastic Foams*. Plastic and Polymer Thechnology, 2016. **4**: p. 11.
23. McCallum, T.J., *Properties and Foaming Behaviour of Thermoplastic Olefin Blends Based on Linear and Branched Polypropylene*, in *Department of Chemical Engineering*. 2007, PhD Thesis, Queen's University: Kingston, Ontario, Canada.
24. Taki, K., et al., *Bubble coalescence in foaming process of polymers*. Polymer Engineering & Science, 2006. **46**(5): p. 680-690.
25. Leung, S.N.S., *Mechanisms of Cell Nucleation, Growth, and Coarsening in Plastic Foaming: Theory, Simulation, and Experiment*. 2010, PhD Thesis, University of Toronto.
26. Yanagisawa, N. and R. Kurita, *In-situ observation of collective bubble collapse dynamics in a quasi-two-dimensional foam*. Scientific Reports, 2019. **9**(1): p. 5152.
27. Bhakta, A. and E. Ruckenstein, *Decay of standing foams: drainage, coalescence and collapse*. Advances in Colloid and Interface Science, 1997. **70**: p. 1-124.
28. Weaire, D. and S. Hutzler, *The Physics of Foams*. 1999, Oxford University Press: New York.
29. Schramm, L.L. and F. Wassmuth, *Foams: Basic Principles*, in *Foams: Fundamentals and Applications in the Petroleum Industry*. 1994, American Chemical Society. p. 3-45.
30. Weaire, D., et al., *The fluid dynamics of foams*. J. Phys.: Condens. Matter, 2003. **15**: p. 953-898454650.
31. Zhang, X.D., et al., *Role of Silicone Surfactant in Flexible Polyurethane Foam*. Journal of Colloid and Interface Science, 1999. **215**(2): p. 270-279.
32. Khatib, Z.I., G.J. Hirasaki, and A.H. Falls, *Effects of Capillary Pressure on Coalescence and Phase Mobilities in Foams Flowing Through Porous Media*. SPE Reservoir Engineering, 1988. **3**(03): p. 919-926.
33. Wasan, D.T., et al., *Foams, thin films and surface rheological properties*. Progress in Surface Science, 1992. **39**(2): p. 119-154.
34. Lobos, J., et al., *Improving the stability of polylactic acid foams by interfacially adsorbed particles*. Polymer Engineering & Science, 2016. **56**(1): p. 9-17.
35. Ruinaard, H., *Elongational Viscosity as a Tool to Predict the Foamability of Polyolefins*. Journal of Cellular Plastics - J CELL PLAST, 2006. **42**: p. 207-220.
36. Lee, S.T., *Foam Extrusion Principles and Practice*. 2000: Technomic.
37. Laguna-Gutierrez, E., et al., *Improving the extensional rheological properties and foamability of high-density polyethylene by means of chemical crosslinking*. Journal of Cellular Plastics, 2018. **54**(2): p. 333-357.
38. Zhai, W., et al., *Cell coalescence suppressed by crosslinking structure in polypropylene microcellular foaming*. Polymer Engineering & Science, 2008. **48**(7): p. 1312-1321.
39. Yu, B., et al., *Internal Application Evaluation of New Experimental OBC-Based Midsole Foam Performance*. 2016 Dow CRI Report - 2016073780.
40. Liu, J., et al., *Study on the Properties of EVA/POE and EVA/OBC Based Foams for Midsole Application*. Dow CRI Report - 2012012755.
41. Gao, Y., K. Kummer, and L. Chen, *Assessment of low levels of INFUSE(TM) OBCs in Cross Linked EVA Foams*. 2014, Dow CRI Report - 2014000533.
42. Kummer, K., B. Yu, and C. Wang, *Comparison of Foam Performance among EVA and Developmental Polyolefin Elastomer Blends*. 2018, Dow CRI Report - 2018002372.

43. Anfu, G., et al., *Effect of microstructure on the properties of polystyrene microporous foaming material*. e-Polymers, 2020. **20**(1): p. 103-110.
44. Niu, Y.-h., et al., *Crosslinking kinetics of polyethylene with small amount of peroxide and its influence on the subsequent crystallization behaviors*. Chinese Journal of Polymer Science, 2016. **34**(9): p. 1117-1128.
45. Tamboli, S., S. Mhaske, and D. Kale, *Crosslinked polyethylene*. Indian Journal of Chemical Technology, 2004. **11**.
46. Poongavalappil, S., et al., *Cross-linking kinetics study and high temperature mechanical properties of ethylene–octene copolymer (EOC)/dicumylperoxide(DCP) system*. European Polymer Journal, 2011. **47**(10): p. 1949-1955.
47. Shinkai, K., N. Chiba, and Y. Ozaki, *Foamable and Crosslinkable Polyethylene Composition, Precess for its Production, and Process for Producing Crosslinked Polyethylene Foams using Said Composotion*, S.C. Co., Editor. 1977: Japan.
48. Sen, A.K., et al., *Kinetics of silane grafting and moisture crosslinking of polyethylene and ethylene propylene rubber*. Journal of Applied Polymer Science, 1992. **44**(7): p. 1153-1164.
49. Rubinstein, M., Colby, R.H., *Polymer physics*, 2003, Oxford University Press.
50. Mezger, T.G., *The Rheology Handbook: For Users of Rotational and Oscillatory Rheometers*. 2006: Vincentz Network.
51. Laguna Gutiérrez, E., *Understanding the Foamability of Complex Polymeric Systems by using Extensional Rheology*. 2016, PhD Thesis, Universidad de Valladolid.
52. Verbrugge, T., et al., *Chemorheology of ultra-fast curing epoxy systems - Part 1. Method development*. Dow CRI Report - 2012013055
53. Gendron, R. and C. Vachon, *Effect of Viscosity on Low Density Foaming of Poly(Ethylene-Co-Octene) Resins*. Journal of Cellular Plastics, 2003. **39**(1): p. 71-85.
54. Vervoort, S. and T. Karjala, *Rheology with application to polyolefins: oscillatory shear and elongational rheology*. 2020, Dow ER20192627
55. Sugimoto, M., et al., *Melt Rheology of Polypropylene Containing Small Amounts of High-Molecular-Weight Chain. 2. Uniaxial and Biaxial Extensional Flow*. Macromolecules, 2001. **34**(17): p. 6056-6063.
56. Sugimoto, M., et al., *Melt rheology of polypropylene containing small amounts of high molecular weight chain. I. Shear flow*. Journal of Polymer Science Part B: Polymer Physics, 2001. **39**(21): p. 2692-2704.
57. Gotsis, A.D., B.L.F. Zeevenhoven, and A.H. Hogt, *The effect of long chain branching on the processability of polypropylene in thermoforming*. Polymer Engineering & Science, 2004. **44**(5): p. 973-982.
58. Laguna-Gutierrez, E., et al., *Understanding the foamability and mechanical properties of foamed polypropylene blends by using extensional rheology*. Journal of Applied Polymer Science, 2015. **132**(33).
59. Spitael, P., & Macosko, C., *Strain hardening in polypropylenes and its role in extrusion foaming*. Polymer Engineering and Science, 2004. **44(11)**: p. 2090-2100.
60. Spitael, P., Macosko, CW, Sahnoune, *Extensional rheology of polypropylene and its effect on foaming of thermoplastic elastomers*. Proc Ann Tech Conf (ANTEC), 2002: p. 1792–1796.

Appendix

A Reaction kinetics

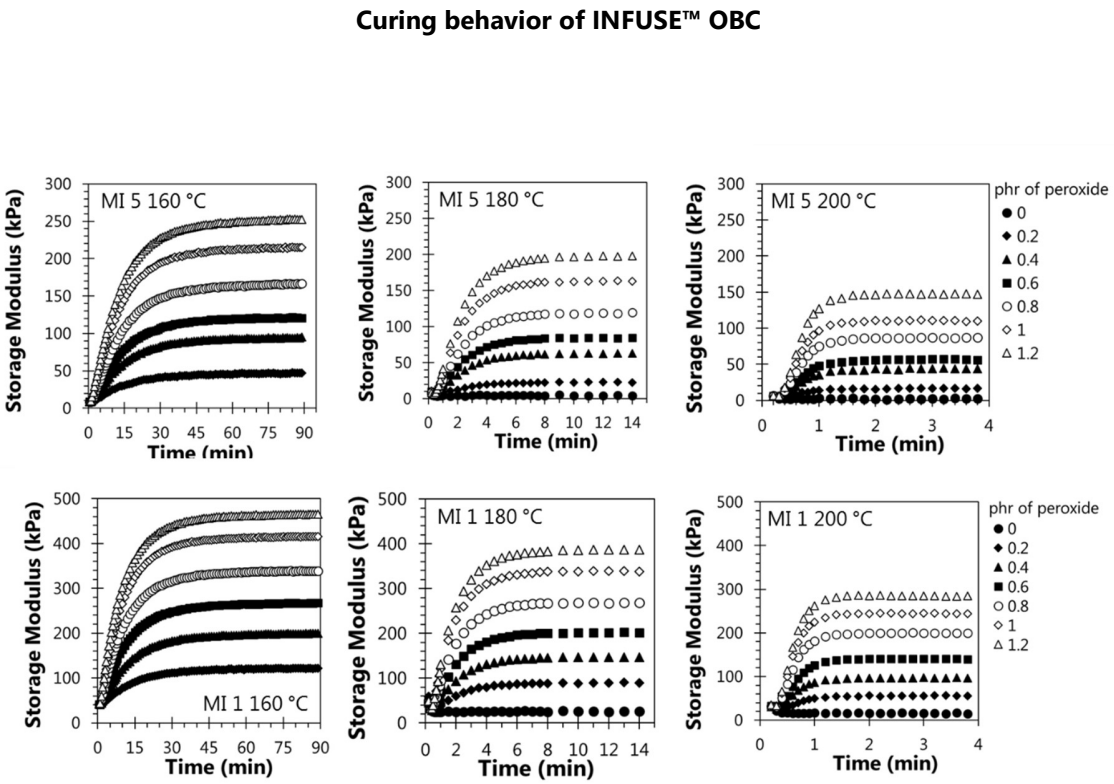

Figure 49: Curing curves of INFUSE 9500 and 9100 compounded with different levels of peroxide at 160, 180 and 200 °C

B Shear Rheology

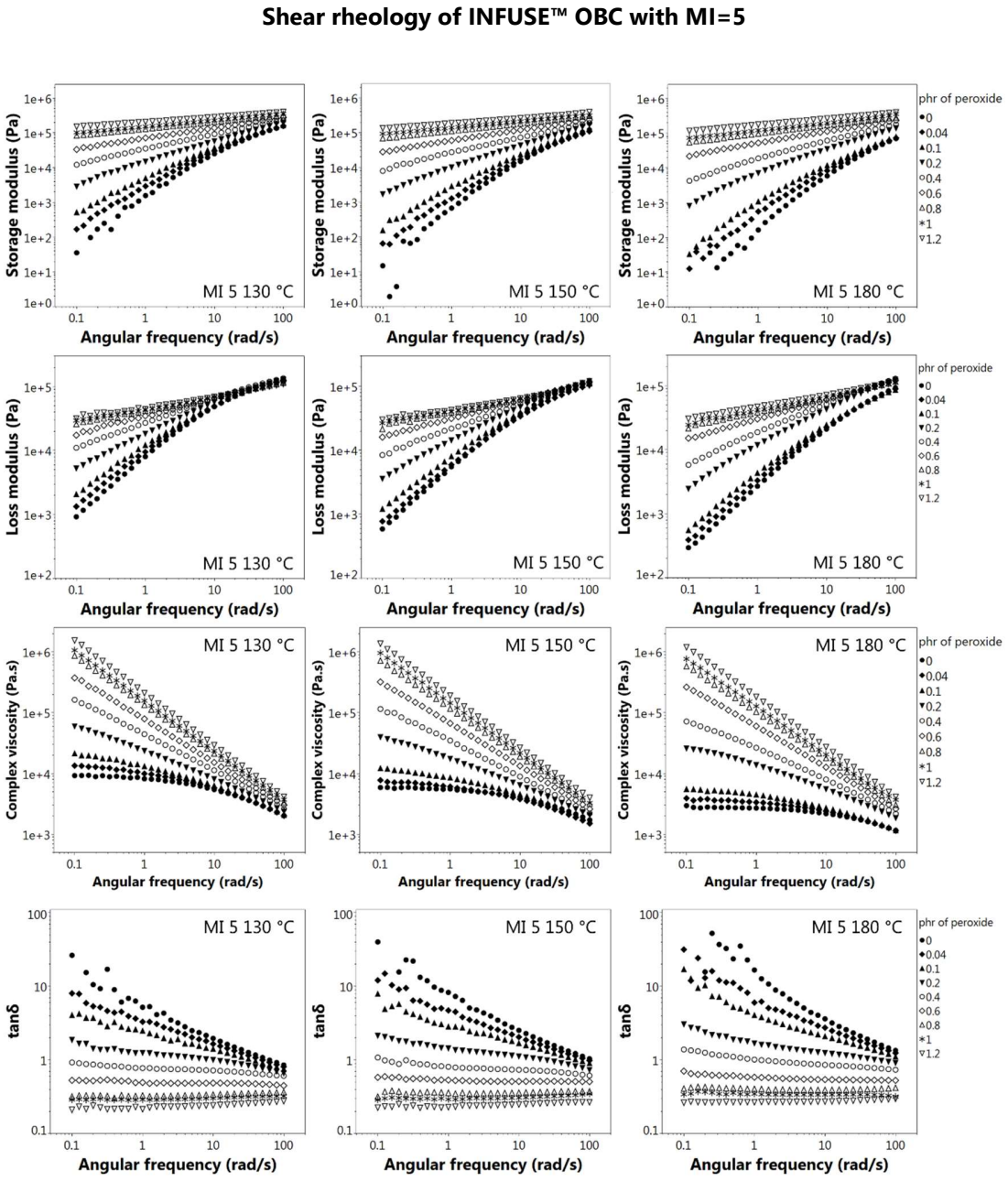

Figure 50: DMA data of INFUSE™ 9500 at 130, 150 and 180 °C modified with different levels of dicumyl peroxide. Data was measured at a suitable angle in the linear viscoelastic regime of the specific compound.

Shear rheology of INFUSE™ OBC with MI=1

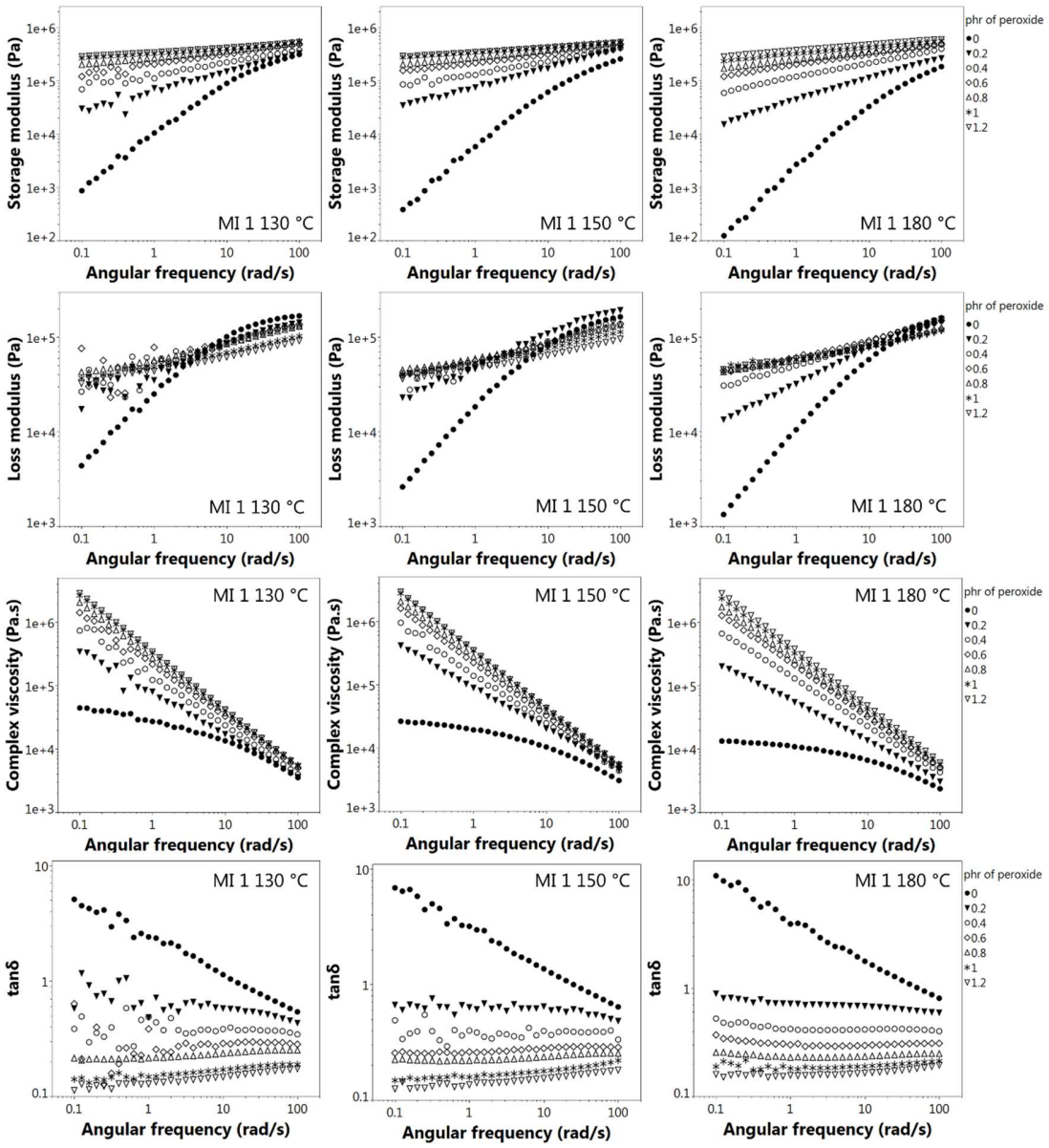

Figure 51: DMA data of INFUSE™ 9100 at 130, 150 and 180 °C modified with different levels of dicumyl peroxide. Data was measured at a suitable angle in the linear viscoelastic regime of the specific compound.

C Extensional rheology

Extensional rheology of INFUSE™ OBC with MI=5

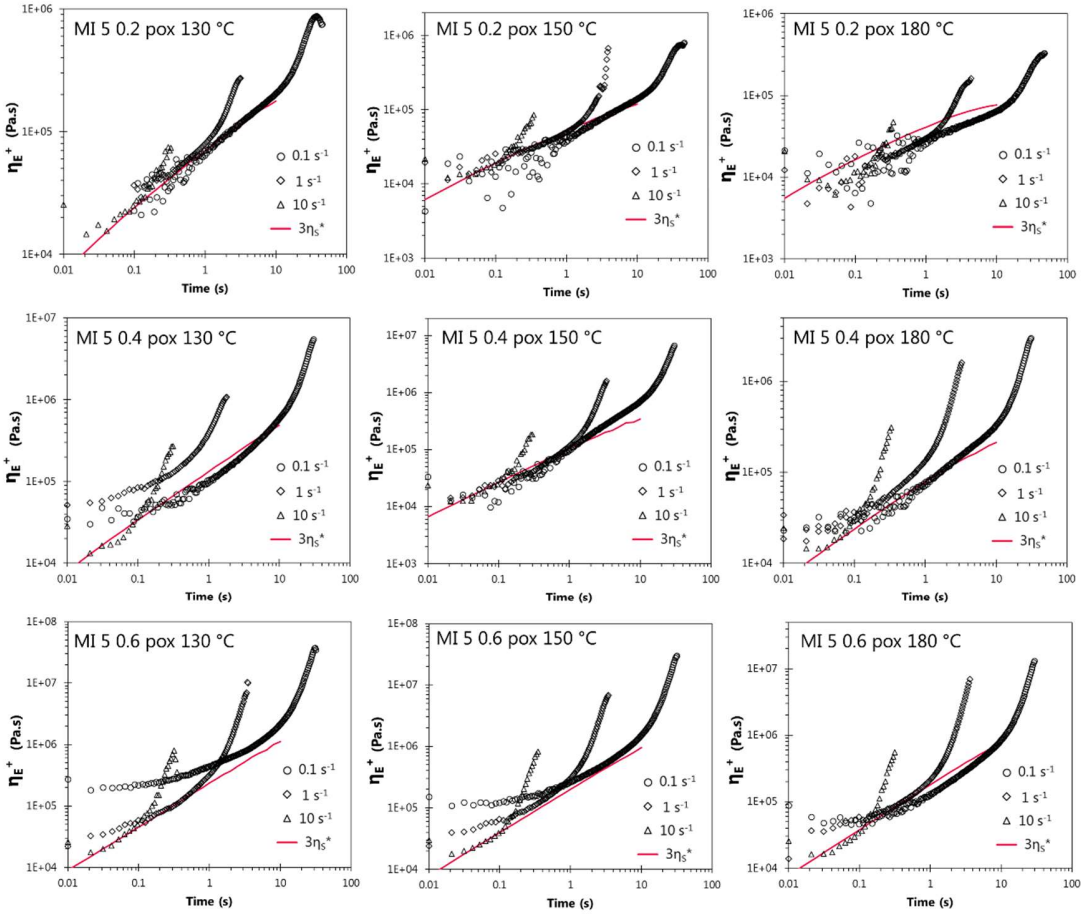

Figure 52: Extensional rheology of INFUSE™ 9500 at 130, 150 and 180 °C modified with different levels of dicumyl peroxide

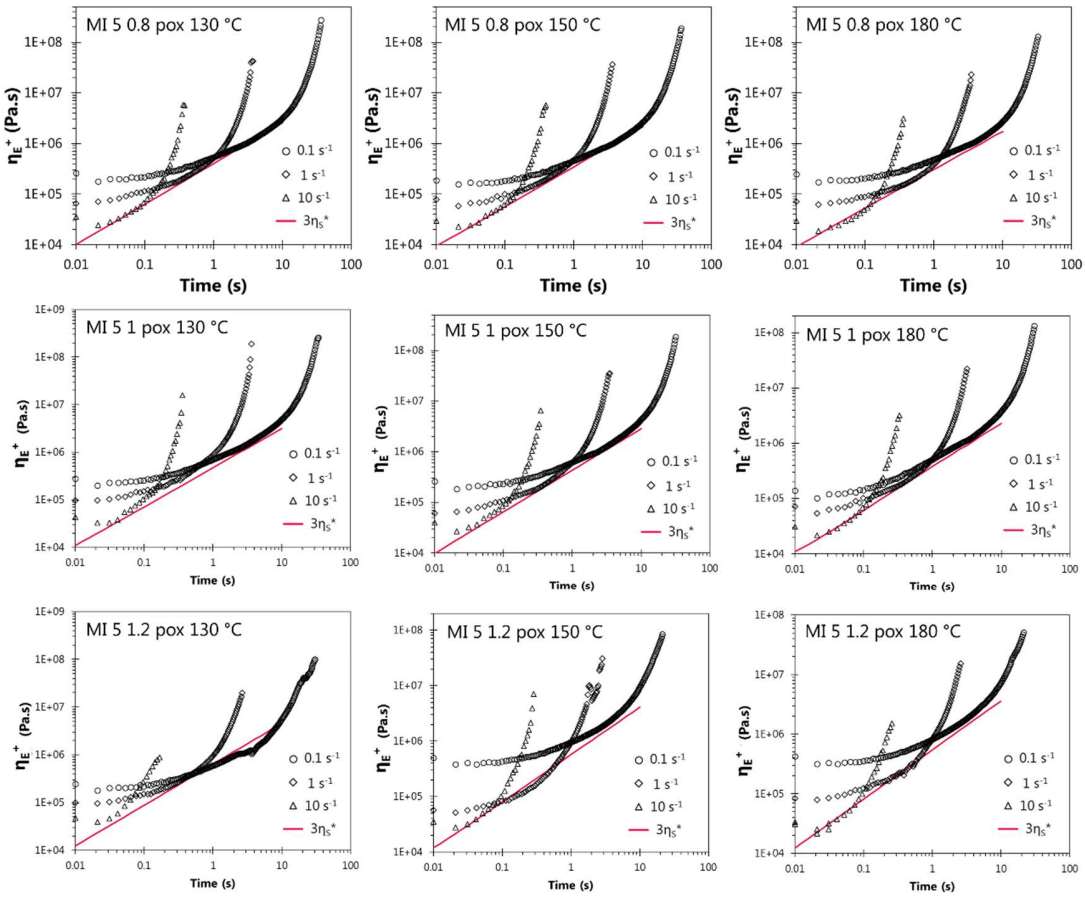

Figure 53: Extensional rheology of INFUSE™ 9500 at 130, 150 and 180 °C modified with different levels of dicumyl peroxide

Extensional rheology of INFUSE™ OBC with MI=1

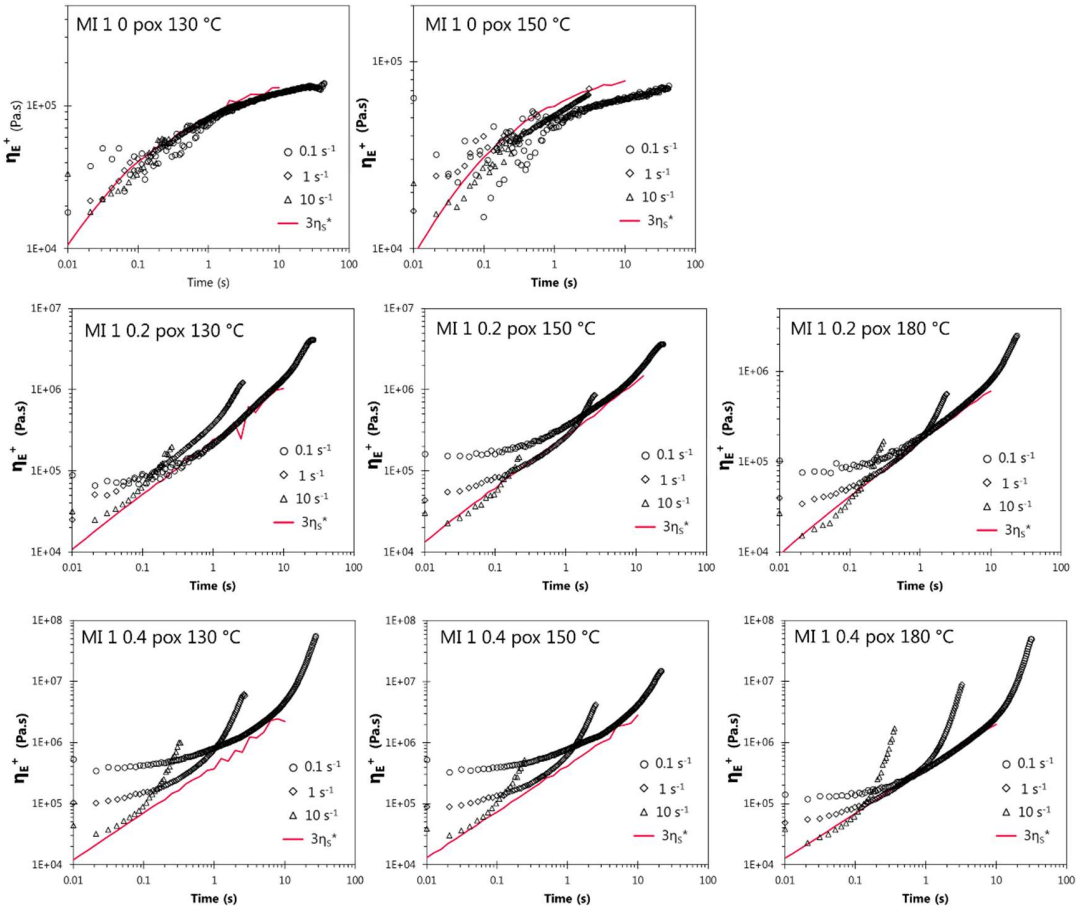

Figure 54: Extensional rheology of INFUSE™ 9100 at 130, 150 and 180 °C modified with different levels of dicumyl peroxide

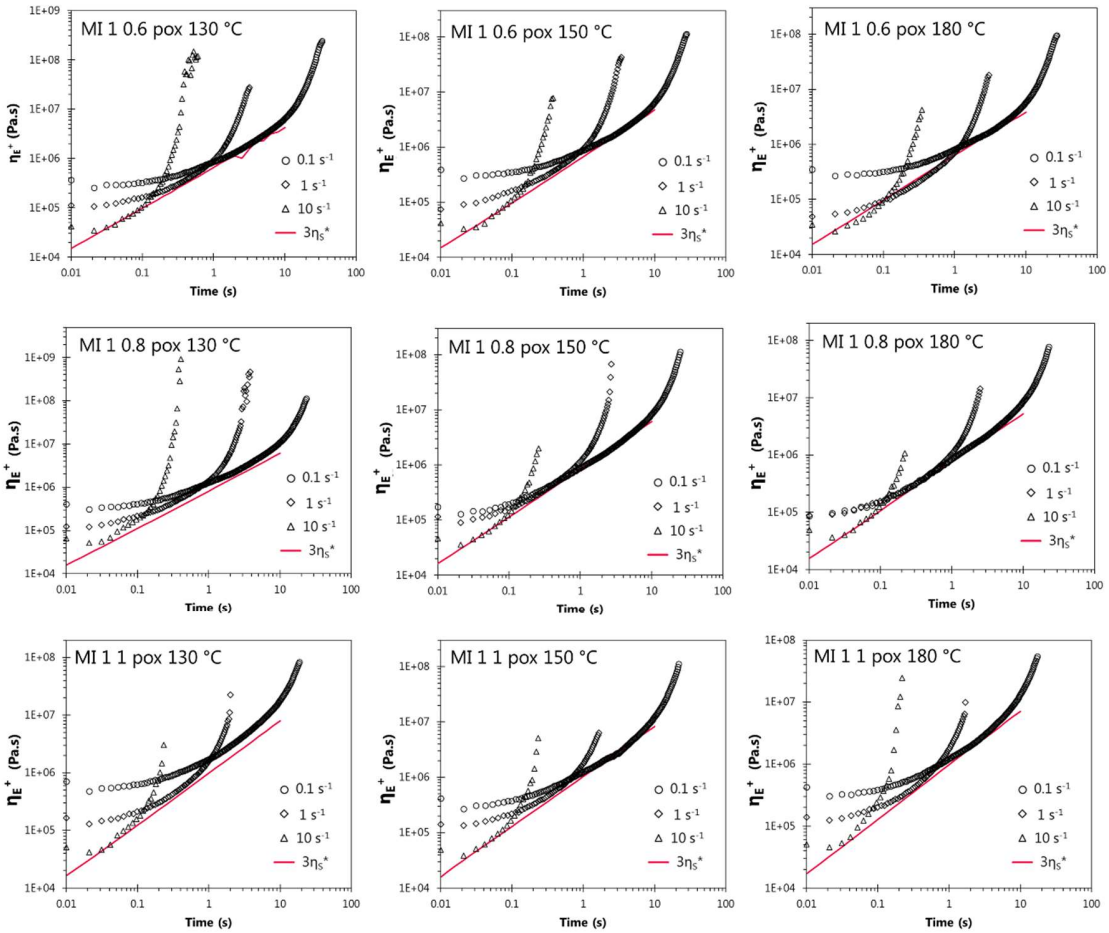

Figure 55: Extensional rheology of INFUSE™ 9100 at 130, 150 and 180 °C modified with different levels of dicumyl peroxide

Strain at break

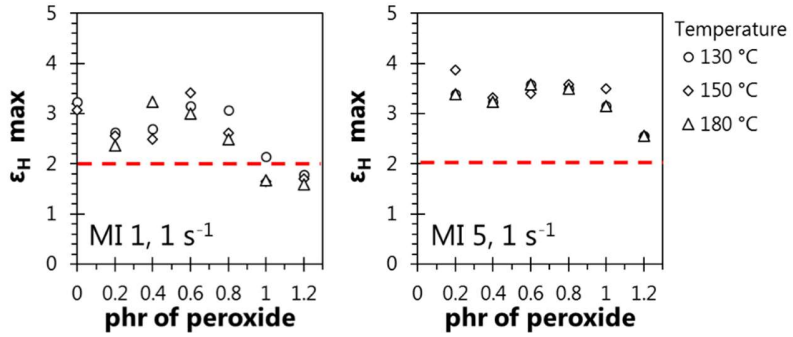

Figure 56: Maximum Hencky strain at a strain rate of 1 s^{-1}. The red dashed line represents the relevant Hencky strain for foaming. All samples of which the maximum Hencky strains drop below the red dashed line could not be represented in relation to foaming.

Strain hardening index

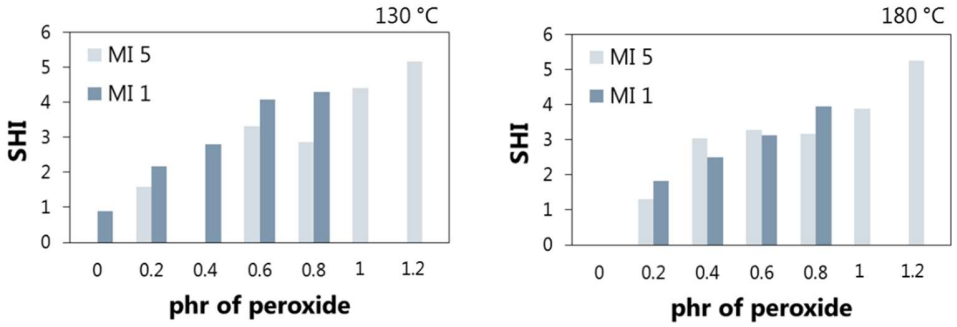

Figure 57: Strain hardening index at a Hencky strain of 2 and a strain rate of 1 s^{-1} at 130 °C and 180 °C

D Cell analysis

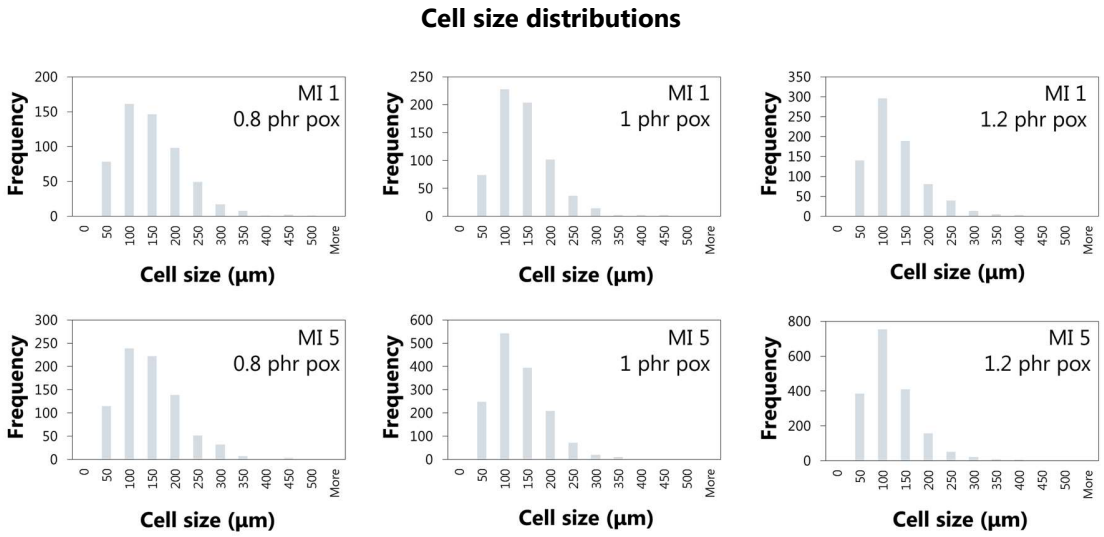

Figure 58: Histograms of cell size distributions of crosslinked injection molded samples.

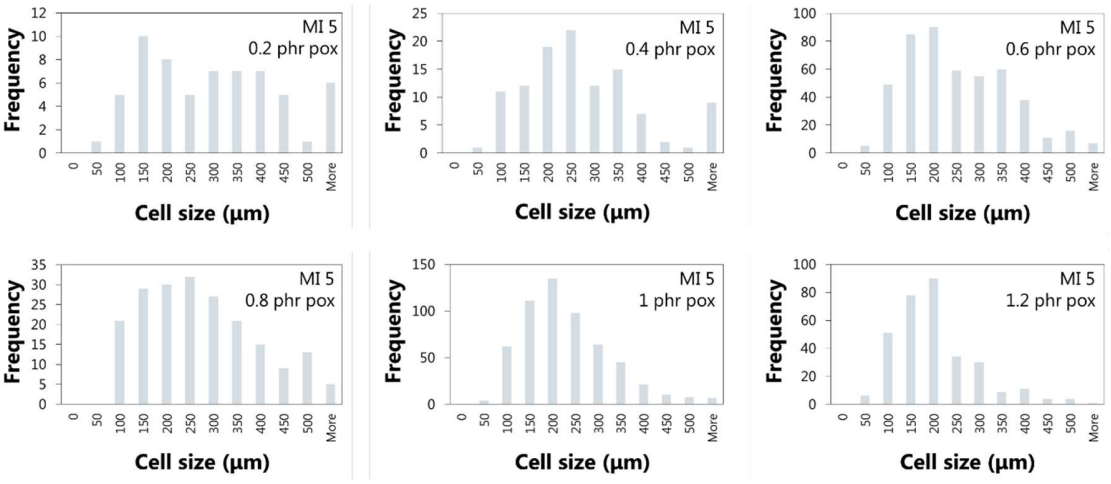

Figure 59: Histograms of cell size distributions of One to One foamed samples.

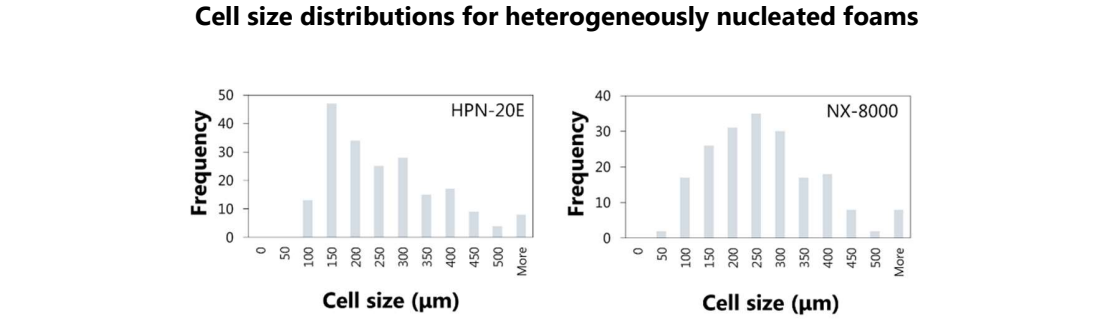

Figure 60: Cell size distributions of samples with and without added nucleating agent. Samples were compounded according to **Table 4** with 0.8 phr of peroxide and two different nucleating agents.

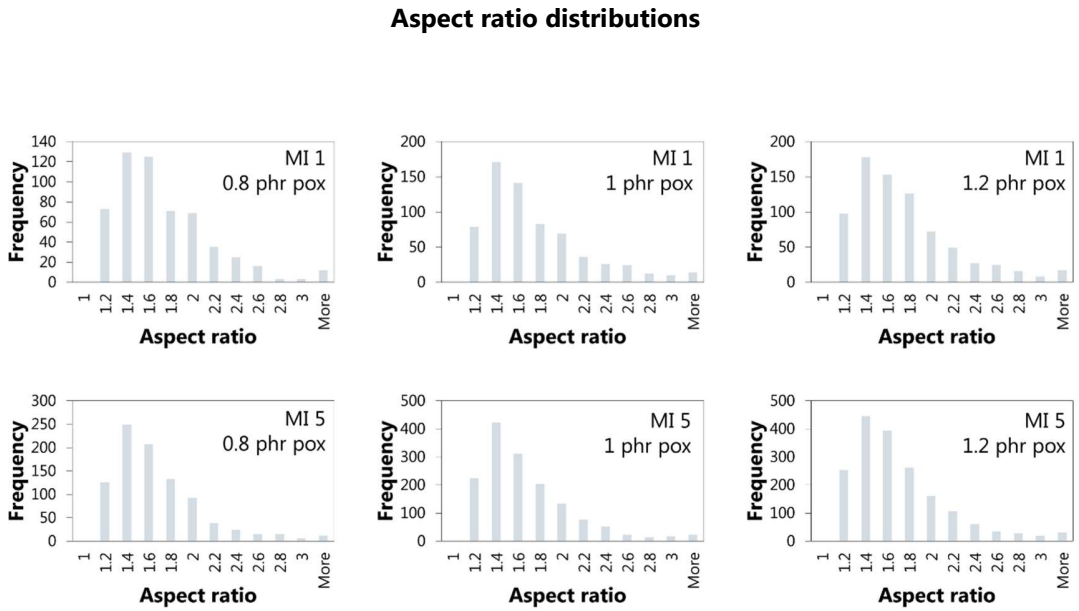

Figure 61: Histograms of the aspect ratio distribution of crosslinked injection molded samples.

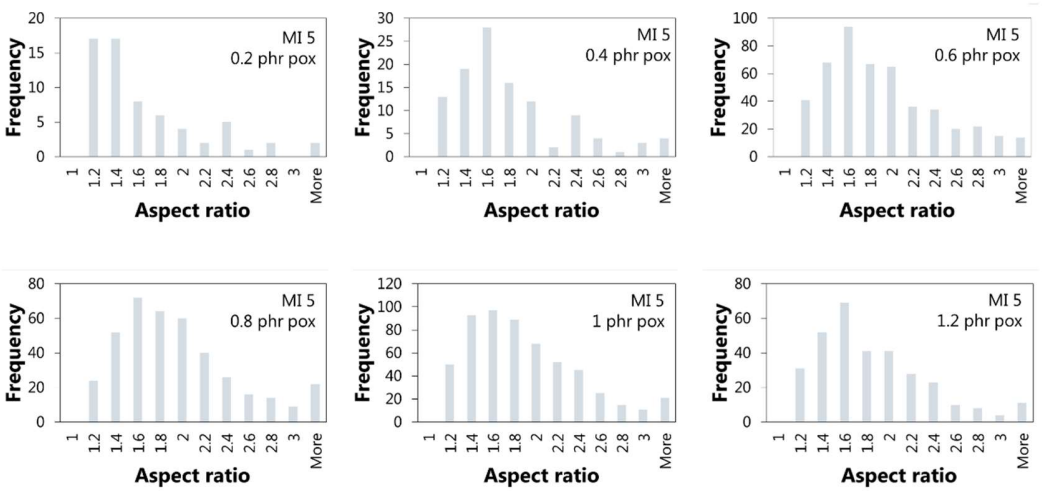

Figure 62: histograms of the aspect ratio distribution of One to One foamed samples.

Table 8: Average aspect ratios for CIM samples

Sample	Average Aspect ratio	Standard deviation
MI 1		
0.8 phr peroxide	1.63	0.46
1 phr peroxide	1.65	0.49
1.2 phr peroxide	1.66	0.50
MI 5		
0.8 phr peroxide	1.58	0.43
1 phr peroxide	1.58	0.45
1.2 phr peroxide	1.61	0.48

Table 9: Average aspect ratios for One to One foamed samples

Sample	Average aspect ratio	Standard deviation
MI 5		
0.2 phr peroxide	1.61	0.61
0.4 phr peroxide	1.72	0.55
0.6 phr peroxide	1.82	0.59
0.8 phr peroxide	1.88	0.57
1 phr peroxide	1.82	0.54
1.2 phr peroxide	1.77	0.55

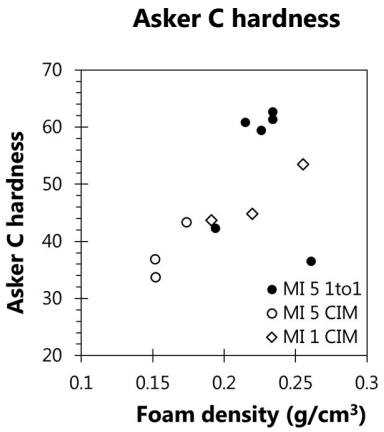

Figure 63: Asker C hardness. One to One foamed samples were measured with skin, Crosslinked injection molded samples were measured without skin.